

AUTOMATED ROOF GENERATION FOR THE CITY OF OLOMOUC USING ESRI CITYENGINE

MASTER'S THESIS

submitted in partial fulfillment of the requirements for the degree
of

Master of Science (MSc)

**PARIS-LODRON UNIVERSITY SALZBURG
(PLUS)**

Faculty of Digital and Analytical Sciences

Department of Geoinformatics

and

PALACKÝ UNIVERSITY OLOMOUC (UPOL)

Faculty of Science

Department of Geoinformatics

PLUS supervisor: Dr. Dirk Tiede

UPOL supervisor: Dr. Stanislav Popelka

submitted by

EKANAYAKA MUDIYANSELAGE RUCHIRA DULANJITH,

EKANAYAKA

Salzburg & Olomouc, May 2024

With the support of Erasmus+ programme of the European Union. This Master's Thesis has been developed in the framework of the Erasmus Mundus Joint Master Degree (EMJMD) "Copernicus Master in Digital Earth", jointly coordinated by Paris-Lodron University Salzburg, Department of Geoinformatics, Austria together with University of South Brittany, Computer Science Department, France and Palacký University Olomouc, Department of Geoinformatics, Czech Republic.

ANNOTATION

Cities attract individuals for a variety of reasons, including job possibilities and economic growth potential. As a result, the complex spatial dynamics of urban settings provide novel obstacles to efficient urban planning. However, typical two-dimensional representations frequently fail to capture the intricacies of three-dimensional systems, making informed decision-making difficult. As Czech cities grow and face new issues, there is an increasing demand for creative 3D modelling approaches. Esri CityEngine provides a viable answer by allowing the production of reusable CGA scripts while also improving the quality and speed of 3D modelling procedures. The application of this technology in urban contexts has the potential to transform urban planning by offering a better knowledge of urban morphology.

The research illustrates the feasibility of using Esri CityEngine with ArcGIS Pro to create a systematic, user-friendly pipeline for creating LOD2 (Level of Detail 2) models with minimum GIS skills. The pipeline automates the computation of factors such as eave height, ridge height, and certain roof kinds, resulting in a feature layer that can be used in CityEngine to generate automated LOD2 models.

The findings demonstrate the successful construction of LOD2 models for specific research areas while also supporting a simplified processing pipeline that conceals workflow difficulties from users. This created pipeline provides thorough advice to users, from initial data gathering to final accuracy evaluation. The created CGA script now supports simulating 15 of the most popular roof shapes in Czechia.

This study marks a huge step forward in urban modelling and analysis, providing a rigorous and scalable framework for creating LOD2 structures in Olomouc and beyond. In addition to addressing current difficulties in building generation, this study provides the framework for future improvements in the area using sophisticated GIS technology and computational tools.

KEYWORDS

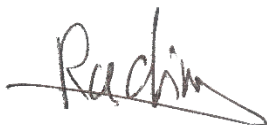
Urban Modelling, BIM, ArcGIS, LiDAR, LOD2

Number of pages 61

Number of appendixes 3

This thesis has been composed by Ekanayaka Mudiyansele Ruchira Dulanjith, Ekanayaka for the Erasmus Mundus Joint Master's Degree Program in Copernicus Master in Digital Earth for the academic years 2022/2023 and 2023/2024 at the Department of Geoinformatics, Faculty of Natural Sciences, Paris Lodron University Salzburg, and Department of Geoinformatics, Faculty of Science, Palacký University Olomouc.

Hereby, I declare that this piece of work is entirely my own, the references cited have been acknowledged and the thesis has not been previously submitted to the fulfilment of the higher degree.

A handwritten signature in black ink, appearing to read 'Ruchira', with a long horizontal stroke extending to the right.

E.M.R.D Ekanayaka

ACKNOWLEDGMENT

I would like to thank my supervisor, RNDr. Stanislav Popelka, Associate Professor Dr. Dirk Tiede for their steadfast support, positive counsel, and insightful input during this journey. Your knowledge and support have really enhanced my research experience, and I am thankful for the opportunity to learn from you both.

To my lovely wife, Sandani Piyasena, who has provided me with constant love and support while being away from home for two years. Your tolerance, understanding, and support have given me strength and motivation. Your unfailing faith in me has been a guiding light through the trials of academics, and I will be eternally thankful for having you in my life.

I would want to convey my heartfelt thanks to my parents for their unfailing love, everlasting support, and unwavering trust in me. Your tireless efforts and constant support have laid the groundwork for my academic success. From instilling in me a love of learning to providing constant encouragement through every success and setback, your advice has shaped me into the person I am today. I really appreciate all you have done for me.

This thesis could not have been completed without the assistance and encouragement of these individuals. Thank you for being a part of this adventure.

Palacký University Olomouc
Faculty of Science
Academic year: 2023/2024

ASSIGNMENT OF DIPLOMA THESIS

(project, art work, art performance)

Name and surname: **Mudiyanselage Ruchira EKANAYAKA**
Personal number: **R220765**
Study programme: **N0532A330010 Geoinformatics and Cartography**
Work topic: **Automated roof generation for the city of Olomouc using Esri City Engine**
Assigning department: **Department of Geoinformatics**

Theses guidelines

The aim of the thesis is to explore methods for roof construction in the city of Olomouc. The student will delve into techniques to estimate roof and building heights, potentially using the digital surface model (DSM) and digital terrain model (DTM). Then, he will develop an approach for the automated creation of roofs using the Esri City Engine. In identifying the shapes of various roof structures, a potential strategy is to utilize high-resolution Lidar point clouds. The research will encompass three distinct areas, ranging from rural sites to the part of the city's historical center. One of the primary outputs will be a comprehensive methodology for such processes. Additionally, guidelines for future applications will be provided. Lastly, the student will discuss the application of the developed model in relation to Copernicus solar radiation data.

The student will create a website about the thesis following the rules available on the department's website and a poster about the diploma thesis in A2 format. The student will submit the entire text (text, attachments, poster, outputs, input and output data) in digital form on a storage medium and the text of the thesis in two bound copies to the secretary of the department.

Extent of work report: **max. 50 pages**
Extent of graphics content: **as needed**
Form processing of diploma thesis: **electronic**
Language of elaboration: **English**

Recommended resources:

ESRI (2023) CityEngine help—ArcGIS CityEngine Resources | Documentation. Available at: <https://doc.arcgis.com/en/cityengine/latest/help/cityengine-help-intro.htm>.

Gergelova, M.B. et al. (2020) 'Identification of Roof Surfaces from LiDAR Cloud Points by GIS Tools: A Case Study of Lučenec, Slovakia', *Sustainability*, 12(17), p. 6847. Available at: <https://doi.org/10.3390/su12176847>.

Jayaraj, P. and Ramiya, A.M. (2018) '3d citygml building modelling from lidar point cloud data', *The International Archives of the Photogrammetry, Remote Sensing and Spatial Information Sciences*, XLII-5, pp. 175–180. Available at: <https://doi.org/10.5194/isprs-archives-XLII-5-175-2018>.

Kelly, T. (2021) 'CityEngine: An Introduction to Rule-Based Modeling', in W. Shi et al. (eds) *Urban Informatics*. Singapore: Springer (The Urban Book Series), pp. 637–662. Available at: https://doi.org/10.1007/978-981-15-8983-6_35.

Widyaningrum, E. et al. (2018) 'Extraction of building roof edges from lidar data to optimize the digital surface model for true orthophoto generation', *The International Archives of the Photogrammetry, Remote Sensing and Spatial Information Sciences*, XLII-2, pp. 1199–1205. Available at: <https://doi.org/10.5194/isprs-archives-XLII-2-1199-2018>.

Supervisors of diploma thesis: **RNDr. Stanislav Popelka, Ph.D.**
Department of Geoinformatics

Date of assignment of diploma thesis: **December 4, 2023**

Submission deadline of diploma thesis: **May 20, 2024**

L.S.

doc. RNDr. Martin Kubala, Ph.D.
Dean

prof. RNDr. Vilém Pechanec, Ph.D.
Head of Department

Olomouc December 4, 2023

CONTENT

LIST OF ABBREVIATIONS	10
INTRODUCTION	11
1 OBJECTIVES.....	12
2 STATE OF THE ART	13
2.1 The importance of 3D building modelling.....	13
2.2 Study area.....	15
2.2.1 History.....	15
2.2.2 Areas of Interest (AOI)	16
2.3 Building footprint detection.....	17
2.3.1 Definition of building footprint.....	17
2.4 Methods of building footprint detection	18
2.4.1 Manual digitising	18
2.4.2 Algorithms and mathematical modelling	18
2.4.3 Object-based Image Analysis (OBIA)	19
2.4.4 Deep learning.....	20
2.4.5 Existing data sources	21
2.5 Building height detection	23
2.5.1 Definition of building height	23
2.6 Methods of building height detection	24
2.6.1 Deep learning.....	24
2.6.2 Open data sources	24
2.6.3 LiDAR data processing	25
2.7 Roof modelling.....	26
2.8 Software and built-in workflows for 3D modelling	27
2.9 Accuracy assessment of 3D models	29
3 METHODOLOGY.....	31
3.1 Data and software used	31
3.1.1 Data Sources	31
3.1.2 Software and programming languages	31
3.2 Abstract representation of the methodology	32
3.2.1 Stage 1 – Initial data extraction and data processing.....	33
3.2.2 Stage 2 - Building footprint database preparation	33
3.2.3 Stage 3 – Accuracy assessment.....	34
3.2.4 Stage 4 – Develop CGA script in Esri CityEngine	35
3.2.5 Stage 5 – Generate 3D model.....	36
3.2.6 Stage 6- Prepare systematic workflow	36
4 ROOF PARAMETERS CALCULATION	37
4.1 Initial data processing.....	37
4.2 Slope, ridge and eave height calculation	38
4.2.1 Evaluation of roof slope	38
4.2.2 Evaluation of ridge height.....	38

4.2.3	Evaluation of eave height.....	39
4.3	Percentage of pixels in each direction	40
5	CLASSIFICATION OF ROOF TYPES	41
5.1	Classification of flat roofs and pitched roofs.....	41
5.2	Classification of pitched roof types	42
6	GENERATE CGA SCRIPT AND LOD2 MODEL	44
6.1	Modelling roof types	44
6.1.1	Basic roof types.....	44
6.1.2	Complex roof types.....	44
6.3	Implement user interface for user interaction	46
6.4	Generate LOD2 model.....	47
7	ACCURACY ASSESSMENT	49
7.1	Accuracy assessment of ridge height	49
7.2	Accuracy assessment of eave height	51
7.3	Accuracy assessment of roof type classification	53
7.3.1	Residential area	53
7.3.2	Rural area.....	53
7.3.3	City Centre area.....	54
8	IMPLEMENTATION OF THE WORKFLOW.....	55
9	RESULTS	56
9.1	Results of roof parameters calculation.....	56
9.2	Results of the LOD2 model.....	57
10	DISCUSSION	58
11	CONCLUSION	62
	REFERENCES AND INFORMATION SOURCES	

LIST OF ABBREVIATIONS

Abbreviation	Meaning
ALOS	Advanced Land Observing Satellite
ALS	Aerial Laser Scanning
BDT	Background Discriminant Transformation
BIM	Building Information Modelling
CGA	Computer-Generated Architecture
CNN	Convolutional Neural Network
ČÚZK	Czech Office for Surveying, Mapping, and Cadastre
DL	Deep Learning
DSM	Digital Surface Model
DT	Decision Tree
GCP	Ground Control Points
GEOBIA	Geographic Object-based Image Analysis
GIS	Geographic Information System
GUI	Graphical User Interface
LiDAR	Light Detection and Ranging
LOD	Level of Detail 2
MAE	Mean Absolute Error
ML	Machine Learning
MSK	Multi-modal selective kernel
NDSM	Normalized Digital Surface Model
OBIA	Object Based Image Analysis
OSM	OpenStreetMap
PA	Producer's accuracy
RANSAC	Random sample consensus
SfM	Structure from Motion
SVM	Support Vector Machine
TLS	Terrestrial Laser Scanning
UA	User's accuracy
UAV	Unmanned Aerial Vehicle

INTRODUCTION

People are drawn to cities for a variety of reasons, including the promise of jobs and prosperity (National Geographic, n.d.). According to the recent report by the World Bank (2023), the urban population is projected to reach 7 out of 10 people by 2050, with over 80% of global GDP generated in cities, emphasising the potential for sustainable growth through effective urban management, innovation, and increased productivity. According to a report published by UNDESA (2019), the urban population is predicted to go beyond the 6 billion mark, while the rural population is predicted to decrease slightly.

Urbanisation's rapid pace and scope, however, present difficulties in meeting the growing demand for jobs, basic services, affordable housing, and a workable infrastructure, especially for the nearly one billion urban poor who reside in informal settlements. As a result, Cities' physical layout and patterns of land usage can be permanent for many generations, resulting in unsustainable sprawl toward suburbs and exurbs (Liu and Yang, 2015; Al-Bilbisi, 2019). According to the findings of Rahaman, Kalam and Al-Mamun (2023), uncontrolled development in Dhaka City has resulted in a variety of public health problems, including air pollution, insufficient sanitation and water supplies, ineffective waste disposal, overpopulation, slums, and unsuitable housing conditions.

In terms of the Czech Republic, suburbanisation is impacted by several variables, such as changing housing and lifestyle choices, better transportation networks, and economic growth. The growth of residential neighbourhoods and infrastructure construction outside of large cities are clear indicators of the trend. There has been a noticeable increase in migration to Prague East, Prague West, Brno Countryside, and Pilsen's northern and southern districts (Šašek, Hlaváček and Holub, 2019). This has led to an increasing trend of suburbanisation. As a result, the capital city has seen the greatest proportional population loss from migration. Šašek, Hlaváček and Holub (2019) further highlighted that in the Czech Republic, suburbanisation has a considerable influence on dwelling construction; it changes the social environment and outskirts of big cities and causes uneven development in towns with selective growth of certain social and demographic categories.

With its diverse spatial dynamics, urban settings bring unique problems and possibilities for efficient urban planning. Traditional two-dimensional representations frequently fail to capture the complexities of three-dimensional systems, reducing the accuracy needed for informed decision-making (Franz, Scholz and Hinz, 2015). As the Czech cities continue to grow and confront new difficulties, there is a rising demand for innovative 3D modelling techniques. Esri CityEngine provides a potential solution for creating reusable CGA scripts, as well as a tool for improving the quality and efficiency of 3D modelling procedures. The use of this technology in cities has the potential to transform urban planning techniques by providing a more thorough grasp of the city's urban form.

This research intends to investigate the background of 3D building modelling in urban planning, highlighting the unique issues and providing a rationale for using Esri CityEngine to automate roof generation as a step towards efficiently addressing the challenges emphasised above. Furthermore, embracing the broader applicability of 3D models in fields like as history, tourism, and other cultural initiatives improves the discussion by emphasizing their importance outside traditional planning domains. This emphasizes the potential of advanced urban modelling tools to improve not just sustainable urban development, but also cultural understanding and resource allocation.

1 OBJECTIVES

The aim of this thesis is twofold: firstly, to address the existing research gap in the Olomouc region, where there is currently no reusable and automated method for creating a Level of Detail (LOD) 2 model; secondly, to create a Computer-Generated Architecture (CGA) procedural programming script with Esri CityEngine, thereby developing a scalable and transferable model. The goal is not only to enhance the replicability of 3D building modelling in Olomouc but also to check the usability of the generated models for solar energy potential assessments. Through this integrated approach, the research aims to contribute to advancing 3D modelling in Esri CityEngine, providing practical solutions for Olomouc while offering insights applicable to diverse urban environments.

- **Primary objective**

Develop a systematic methodology to automatically generate LOD2 buildings in the city of Olomouc.

- **Specific objectives**

1. Determine the building roof types, roof components and building height.
2. Develop CGI scripts in Esri CityEngine to automate building generation.
3. Accuracy assessment of the generated 3D roof models.
4. Utilize the developed model to estimate solar energy potential.

The scope of this research is defined by its focus on the integration of 3D building modelling methodologies within the context of Olomouc's changing urban landscape, utilising Esri CityEngine as a central technological tool. Geographically, the research is bounded by the urban dynamics of Olomouc, encompassing diverse areas such as the city centre, rural zones, and apartment regions. The temporal scope is constrained by the available data sources, such as LiDAR data and optical imagery published by the State Administration of Land Surveying and Cadastre (ČÚZK).

The results of the work will enrich the multidisciplinary fields of Geographic Information Systems (GIS), 3D building modelling in urban landscapes. The implemented workflow allows users to generate a LOD2 building model, which will open doors for a multitude of applications, including but not limited to 3D visualisation, Solar energy cadastre preparation, noise propagation, et al. research, which is critical in decision-making to resolve intricate problems in an urban environment.

2 STATE OF THE ART

In the forthcoming literature review chapter, several key topics relevant to building modelling are discussed. These include an exploration of the historical development and diverse applications of building modelling, as well as an examination of the accuracy of models produced in various domains. The review will also encompass specific aspects of building modelling, such as building footprint detection, height determination, roof slope analysis, and the identification of roof edges. Additionally, the range of software tools used for building modelling will be analysed, and a literature review will be concluded with an analysis of methods for assessing the accuracy of generated models.

2.1 The importance of 3D building modelling

Based on empirical evidence, the utilisation of 3D modelling in established cities proves to be a highly efficient tool for resolving challenges and enhancing urban planning and development. In a period where we are experiencing an energy crisis, 3D modelling is widely used in estimating solar energy potential research. Chiabrando et al. (2017) highlighted the importance of renewable energy, thus identifying appropriate locations to leverage solar energy. In the study, they utilised digital photogrammetry techniques and tested the available open-source software systems. The results of the analysis indicated that the 3D structures generated from Structure from Motion (SfM) software are accurate enough to match the collected ground truth data. Machete et al. (2018) examined the impact of urban context on buildings' solar energy potential using 3D GIS. The study was conducted on a city block in downtown Lisbon during summer and winter with varying degrees of contextual details. The study also demonstrated the great capability of the 3D approach to fully assess solar energy potential in intricate urban layouts, considering the irradiation of all building surfaces exposed to the sun. While 3D models have proved to be an excellent approach for solar data modelling, Willenborg, Pültz, and Kolbe (2018) argued that its analytical capabilities are limited due to the simple data models. Thus, they proposed a semantic 3D city data model instead of the conventional 3D mesh model. Their approach was applied for a solar potential analysis, which showed a significant increase in estimation quality as a result of mesh integration.

Over several decades, the use of 3D models in noise propagation research has greatly advanced our understanding of **how sound propagates** through complex environments. Hewett (2010) conducted a comprehensive analysis of sound propagation in an urban environment. While the primary goal of the analysis is to examine how sound spreads in urban environments, taking into account elements like energy absorption by walls and the surrounding environment, redistribution at intersections, etc., the study also emphasises how crucial it is to have a three-dimensional model of the city for studies on noise propagation. Deng, Cheng and Anumba (2016) argued that conventional 2D maps fall short of capturing the full spectrum of noise level variations, particularly pronounced in high-rise buildings, where the difference between the first and top floors can be significant; 3D Geographic Information System (GIS) models have emerged as a sophisticated solution for representing real-world traffic noise impact. Another important study on noise propagation was done by Cai, Yao and Wang (2018). They implemented a methodology to simplify the computation-intensive noise propagation tasks in 3D space. They contended that, despite the distance attenuation principle of sound, a building's upper floors should have quieter levels than its lower floors; this is frequently not the case. This disparity results from neighbouring buildings obstructing

noise on the lower floors while leaving the upper floors clear. This emphasises even more how crucial it is to have 3D models available for analysis in noise propagation studies.

Based on empirical evidence, 3D models have proven to be useful not only for addressing noise level variations within multi-story buildings but also for **Urban Planning and Zoning**. As it offer a thorough depiction of urban landscapes, these models are invaluable resources for architects, policymakers, and urban planners. They make it possible to evaluate prospective building projects, visualise already-existing structures, and analyse in three dimensions how these might affect the surrounding area. In the work of Danilina, Slepnev and Chebotarev (2018), they emphasised the detailed reality that the 3D model shows can not only mirror the static state but also be a basis for modelling dynamic processes in different areas of urban life, which includes mobility of vehicles and non-motorized vehicles, emergency escape routing et cetera. Users can now run simulations that let them communicate with the virtual model in a manner similar to what they would do in real life because 3D data and visual representation are available within a 3D city model (Alam, 2011). Examining the urban system at different resolutions or levels of detail can benefit from the enhanced and simplified user interactions provided by 3D models (Allen and Berkley, 1979).

In **emergency response**, 3D building modelling has proven to be an invaluable tool. It is essential for disaster management, preparedness, and quick response times. The ability of first responders, emergency managers, and decision-makers to handle a variety of emergencies - from man-made crises to natural disasters - has been substantially improved by this technology. By combining CCTV data with a 3D model of a city, Hong, Lu and Chen (2019) demonstrated a novel approach that has the potential to go beyond the traditional methods and improve data collection, management, and decision-making during emergency response. Also, Hong and Tsai (2020) suggested a web-based decision support system (DSS) that made use of a 3D building framework. Within the DSS, users could enter hypothetical or actual disaster scenarios, and the system would automatically produce information on damage assessment that could be visualised.

3D modelling has emerged as a strong tool for **tourism and cultural heritage**. Virtual reconstructions may bring historical locations to life, providing immersive experiences for both tourists and academics. These models enable the safeguarding and documentation of historic buildings, as well as in-depth explorations of ancient cultures and historical events. In addition, 3D models are important educational materials, offering interactive platforms for learning about other cultures and locations.

In summary, 3D building models have shown to be an incredibly useful and adaptable tool in a variety of fields. 3D models have proven invaluable in a variety of applications, from improving our understanding of noise propagation and its effects on urban environments to optimising solar energy harnessing through precise shading analysis. Furthermore, they have helped make well-informed decisions and contributed to the development of more sustainable and peaceful cities in the field of urban planning and zoning. Their importance is further highlighted by the fact that they help allocate resources, enhance disaster preparedness, and offer situational awareness when it comes to emergency response activities. The empirical data exhibited in these four applications highlights the significant influence of 3D building models on various domains, rendering them a priceless resource for scholars, decision-makers, and practitioners in search of data-driven solutions.

2.2 Study area

Olomouc is a significant city in Moravia and the administrative centre of the Olomouc region. It is the country's sixth biggest city and the most significant city in Moravia's Haná area. Its well-preserved Old Town is one of the most picturesque in the country. Although it receives many local and international tourists, the city nevertheless appears to be underrated.

2.2.1 History

Thousands of years ago, prehistoric humans explored the region where Olomouc now stands, and archaeological findings reveal that the ancestors of today's Olomouc residents have roots dating back to the Stone Age (Holpuch, n.d.). The fertile local soil supported early agricultural activities, attracting both Celtic and Germanic settlers (Information Centre Olomouc, n.d.). Notably, the Romans established a military camp in Neředín in the second half of the second century AD, strategically positioned during conflicts with the Marcomanni, marking the northernmost evidence of Roman presence in Central Europe (Holpuch, n.d.).

Olomouc's architecture is a wonderful combination of historical styles from different ages. It is home to a wealth of architectural marvels dating back to the medieval period and continuing through the Baroque and Renaissance. The city's historic centre is made up of lovely cobblestone lanes flanked by vivid façades of Gothic, Renaissance, and Baroque buildings (Radio Prague International, 2012). The Town Hall, with its elegant tower and exquisite paintings, is a fine example of the Renaissance style and serves as the centre of the main plaza. Figure 1 demonstrates some of the significant historical attractions.

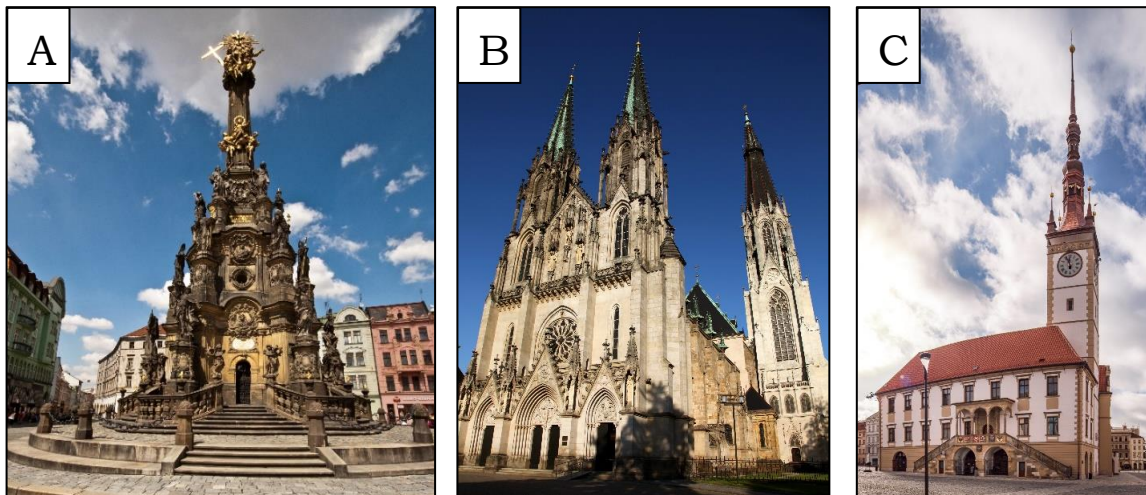


Figure 1: Attractions in Olomouc (A. Column of Holy Trinity; B. St Wenceslas' Cathedral; C. Town hall)

However, there were difficulties throughout this time, as Olomouc lost its university for almost eight decades, only to be restored after World War II (Palacký University Olomouc, n.d.). Nonetheless, the city suffered difficulties under both Nazi and Communist totalitarian governments, which resulted in the destruction of the synagogue and the erection of prefabricated housing. Olomouc saw a terrible flood in 1997, which was paired with the designation of the Baroque Column of Honour of the Holy Trinity as a UNESCO World Heritage Site, demonstrating the city's perseverance in the face of both natural

catastrophes and historical trials, especially during the 1713 – 1715 plague (UNESCO, 2000).

2.2.2 Areas of Interest (AOI)

Figure 2 depicts three research areas of varying complexity. Accordingly, the city centre represents the most complex with different architectural and roof structures, while the rural region has more semidetached dwellings. Finally, in residential area, most structures consist of apartment complexes with flat roofs.



Figure 2 Selected study areas for the analysis

2.3 Building footprint detection

In 3D building modelling, the identification of building footprints is crucial since it serves as the basis for many important applications. Precise building footprints guarantee that 3D models accurately depict actual structures, which makes infrastructure development, zoning, and urban planning easier. Many techniques have been used for building footprint detection over time, which reflects how data sources and technology are always changing. With the increasing complexity and accuracy of these methods, it is now possible to detect building footprints in a variety of contexts with greater accuracy and efficiency. The empirical studies indicate three main ways of delineation of building footprints (manual, semi-automated and automated).

2.3.1 Definition of building footprint

The term "building footprint" takes on diverse definitions depending on the specific application or the thematic focus of the study. According to Lawinsider (n.d.), the horizontal area visible on a plan, measured from the outer borders of all external walls and supporting columns, is known as the building footprint; moreover, It includes houses and connected garage spaces larger than 200 square feet; however, it does not include detached garages, carports and other auxiliary structures. In the field of construction, building footprint refers to the extent of the ground occupied by the building (ECC, n.d). Several institutions and researchers also defined the building footprint in various ways. Biljecki et al. (2021) mentioned that building footprint is depicted as complete blocks, whole buildings, building components, or, in certain circumstances, numerous levels; however, he further emphasised that it is sometimes ambiguous and may change between areas, which can lead to interoperability challenges and noisy findings in large-scale models. Figure 3 demonstrates the captured building footprint by Ecopia Building Footprint – DigitalGlobe.



Figure 3: Capturing building footprint - Source: DigitalGlobe (2017)

2.4 Methods of building footprint detection

2.4.1 Manual digitising

Manual digitising of building footprints is one of the oldest methods of extracting building footprints from high-resolution remotely sensed images, which involves moving a digitiser on captured features (Huang and Liu, 1997).

Manual on-screen digitisation can be an extremely labour- and time-intensive process. Building footprints can be distinguished without a high degree of expertise, but the operator's level of experience does influence how quickly the digitisation process moves along. Even though it can be used across a large city, the time required for digitisation in the application of Building Information Modelling (BIM) is labour-intensive and time-consuming (Wang, Cho and Kim, 2015; Bassier, Vergauwen and Van Genechten, 2017; Paliwal *et al.*, 2021). Having several GIS operators split up the work and compile the results at the end could help with scalability. With this approach, you have complete control over the outcome and can achieve the highest level of accuracy in your digitised building footprints.

Over the years, many researchers compared manual digitising with other approaches to building footprint extraction. Sahin *et al.* (2008) conducted a study to compare feature extraction using Object Based Image Analysis (OBIA) and manual digitising. They conducted a comprehensive analysis involving the manual digitisation of building boundaries and road centrelines juxtaposed with the object-oriented classification process within the same geographical area. The study area encompassed both orderly and disordered zones, discerning between areas constituted by buildings and independent houses. The results indicated that both methods possess inherent drawbacks. Overall, they concluded that the OBIA method could not achieve the anticipated accuracy; thus, the manual method is more accurate in comparison to the OBIA approach.

Sahar and Faust (2013) also conducted a combined approach which involve manual digitising and utilising GIS parcel layers. In this study, they used parcel geometry to locate building locations, which was followed by manual or automatic extraction. Later, they compared the results using the following approaches: 1- Fully manual (Manual digitising from the entire scene), 2- Simplified manual (Manual digitisation following the simplification process). They emphasised that the manual procedure is simplified to provide a pragmatic approach, which relieves the arduous task of manually digitising buildings of any kind from imagery by localising the extraction to a relatively small area.

2.4.2 Algorithms and mathematical modelling

Over the years, numerous well-known methods and algorithms for building and urban mapping have been introduced. These developments have been essential in helping to solve the problems brought on by the growing scale and complexity of urban environments.

Michelin, Mallet and David (2012) implemented a novel 3-step approach to detect building edges. The proposed methodology is underpinned by the fundamental assumption that buildings can be effectively approximated by polygons, meaning they can be fragmented into segments. Step 1 – building areas are coarsely retrieved and classified into boundary and non-boundary regions; step 2- the 3D boundary segments are estimated using the standard RANSAC algorithm (Fischler and Bolles, 1981); step 3- Boundary adjustment, the last stage of the process, involves fine-tuning the locations of

the 3D segments and supporting 3D points using a physical model. The results indicated that 87% of building edges were detected with 12% of false detection rates. However, they further mentioned that the proposed approach exhibits a primary limitation in that it exclusively considers segments, neglecting the potential inclusion of other primitives, such as circles or curves, that may be more suitable for certain landscapes.

Background Discriminant Transformation (BDT) is also a technique that is used in building extraction. Using BDT, the discriminant function is used to improve the distinction between the background and foreground classes. It works especially well in situations where it is difficult to discern building features from the background. Sohn *et al.* (2005) used this method to reduce the prominence of the background to emphasise the building as a non-background. Later, Hausdorff distance and colour indexing algorithms were adopted to detect building pairs, thereby further enhancing the accuracy by point matching. Finally, 3-D building models were generated by utilising least square image matching. Empirical evidence suggests that the use of BDT in building detection applications has been extremely limited since 2010, with very few publications occurring between 2000 and 2010—the majority of which were written by the same author.

Hough Transformation is another algorithm used for detecting linear structures, such as building edges or outlines. This method has been used in many studies (Overby *et al.*, 2004; Liu, Wang and Liu, 2005; San and Turker, 2010; Cui, Yan and Reinartz, 2012; Li *et al.*, 2018) to extract buildings by identifying the lines that denote building boundaries as it is strong at detecting geometric patterns. San and Turker (2010) used Hough transformation for building extraction using satellite imageries. The results of the study indicated that the average building detection percentages are over 93% for industrial buildings, and residential circular and rectangular buildings are over 78% and 95%, respectively.

Müller and Zaum (2005) utilised a Combination of Geometric (object form and size), Photometric (most frequent and mean hue), and Structural Analysis (shadow and surrounding). It considers the spatial arrangement, radiometric properties, and structural patterns in the building footprint extraction process. The method that is being presented only uses aerial photos to extract buildings. The process starts with the entire image being segmented using a seeded region growing algorithm. Starting from seed points, this algorithm expands regions according to pre-established criteria, thereby clearly defining discrete areas within the aerial imagery.

2.4.3 Object-based Image Analysis (OBIA)

OBIA is an alternative to pixel by pixel approach that uses image objects as fundamental evaluation units (Lang, 2008; Blaschke, 2010). By grouping several pixels into forms with a meaningful representation of the objects, this method intends to avoid the problem of artificial square cells as used in the per-pixel method (Blaschke, 2010). OBIA's goal is to handle more complicated classes defined by spatial and hierarchical relationships both within and outside of the classification process (Lang, 2008; Wienert *et al.*, 2013). OBIA is typically divided into three stages: image segmentation, feature extraction and classification.

Geographic object-based image analysis (GEOBIA) is a modified OBIA approach to remote sensing image analysis that identifies and investigates image-objects: groups of adjacent pixels representing real-world geographical features (Blaschke, 2010). Recent reviews comparing GEOBIA and pixel-based methods showed methodological issues and emphasised how GEOBIA surpasses the pixel-based methodology that has been around

for more than three decades, especially for high-resolution imaging (Kucharczyk et al., 2020). The efficacy of using GEOBIA in the application of building footprint extraction has been consistently demonstrated by empirical evidence (Kumar and Bhardwaj, 2020; Prathiba et al., 2020; Zhang, Han and Bogus, 2020; Norman et al., 2021).

The intrinsic heterogeneity of urban environments has limited the accuracy of conventional pixel-based approaches in extracting building footprints, which has led researchers to investigate alternative approaches. In addressing these challenges, the study of Prathiba et al. (2020) employs OBIA as a robust technique for building footprint extraction, specifically utilising Cartosat-2 series data. The synergy of supervised nearest-neighbour classification decision rules had yielded a compelling result demonstrating an accuracy surpassing 82.5% in building footprint extraction. The work of Zhang, Han and Bogus (2020) also shows the applicability of OBIA in building footprint extraction in three different study areas. In this work, features such as trees and buildings were extracted using aerial LiDAR data based on height information. Afterwards, trees were separated and eliminated from the identified items using colour-infrared aerial photographs. Then, building footprints were defined using OBIA. The accuracy assessment indicated a success rate of 75% for two study areas and a 50% success rate to detect building footprints in one study area.

Certain studies highlighted the advantage of utilising OBIA rule-based classification methods (decision rules based on object primitives and fuzzy rules) in building footprint extraction. The work of Kumar and Bhardwaj (2020) used a combination of orthoimages along with the Digital Elevation Model (DEM) to create a rule-based classification guided by object primitive and fuzzy rules. The results showed that overall accuracy was higher than 93%, especially in regions with more substantial but sparsely populated structures. On the other hand, regions with denser populations and smaller buildings showed marginally worse overall accuracy. This implies that the suggested method performed exceptionally well in correctly recognising and categorising buildings, especially in areas that were less populated and had larger structures. Another interesting study was conducted by Norman et al. (2021), where they used medium-resolution sentinel 2B images instead of high-resolution images like most studies. They carefully chose features that are essential for building detection and established the appropriate segmentation parameters (scale, shape, and compactness). They used machine learning (ML) algorithms, specifically the Support Vector Machine (SVM) and Decision Tree (DT) classifiers and found that the SVM classifier performed better than the DT classifier, yielding an amazing 93% accuracy with a kappa value of 0.92 and a notable 20% increase in accuracy. This result demonstrates how well applying ML algorithms to improve classification methods in OBIA works, especially for medium-resolution images.

2.4.4 Deep learning

Deep Learning (DL) algorithms have witnessed a remarkable surge in popularity for remote-sensing image analysis over the past few years, revolutionising the field with their capacity to automatically learn hierarchical representations of data. Deep learning's remarkable capacity for hierarchical learning of representative and discriminative features has sparked a fresh wave of exciting work on the processing and analysis of Remote Sensing big data (Chi et al., 2016; Parente et al., 2019; Sedona et al., 2019).

While the remarkable success of DL is highlighted in many studies, there are few studies that emphasise the concerns and challenges of DL methods in terms of data availability and its quality, computational resources, explainability, sensor variability, etc. For training, deep learning models frequently need a lot of labelled data, which can

be hard to come by in remote sensing (Ahmed et al., 2023; Cheng et al., 2023; Janga et al., 2023). In terms of computational resources, deep Neural network training requires a large amount of processing power. Large-scale remote sensing datasets, particularly those obtained at high resolutions, need a robust computer infrastructure to provide effective training and inference (Hong et al., 2021; Cheng et al., 2023; Janga et al., 2023; Safonova et al., 2023). Deep learning models are often considered "black boxes" due to their complex architectures, which raises the question of how much we can trust AI systems if we don't comprehend how they make their decisions (Eschenbach, 2021). DL models trained on data from one remote sensing sensor may not generalise well to data from a different sensor (Wold and Sandin, 2023); thus, Transfer learning techniques are essential for adapting models to various sensors (Donges, 2022).

Despite the mere limitations of the deep learning approach, it has been widely used in BIM-related applications. Recently, Convolutional Neural Networks (CNN) have been successfully applied for building footprint extraction applications. Chafiq et al. (2021) conducted a U-Net-based deep learning approach for building boundary extraction, where it used images captured from a drone. One of the numerous benefits of the model presented in this research is its capacity to provide more precise identification and automated detection of building footprints using the training model. Furthermore, it demonstrates how AI has advanced to the point where it is advantageous to use better ground truth labels for segmentation construction without the need for human participation. Rastogi, Bodani and Sharma (2022) proposed a novel CNN model called UNet-AP, an improved U-Net architecture where they used Cartosat-2 series multi-spectral images to extract building footprints. The outcomes showed that this innovative architecture consistently improves the result and outperforms both SegNet and UNet architectures.

Compared to the aforementioned methods, there are unique approaches that utilise a combination of CNN architecture for automated building footprint extraction. Li *et al.* (2021) proposed a combined architecture that uses U-Net (create segmentation maps), Cascade R-CNN (detection of building bounding boxes) and Cascade CNN (detection of building corners) for each individual step of the process. Later, a Delaunay triangulation method was used to build final building footprints based on the results of the previous steps. Li *et al.* (2022) emphasised that although CNNs provide encouraging results on a smaller scale, one of their typical flaws is that they are unable to precisely identify building borders, which blurs the result. Therefore, Li *et al.* (2022) proposed a novel CNN architecture with two models: 1- Img2AFM (Enhance building surface and suppress background) and 2- AFM2Mask (predict segmentation masks of buildings). They tested the approach in three different datasets and concluded that it performs building detection significantly better than other methods.

2.4.5 Existing data sources

Building footprint data, which outlines the shapes and dimensions of structures, can be sourced from various channels with little to no post-processing. Government open data portals are primary resources, offering building footprint information processed through aerial surveys and satellite imagery. Additionally, geospatial data repositories like OpenStreetMap (OSM) provide collaborative mapping data where users contribute and edit geographical details, including building footprints. Moreover, commercial data providers such as Esri (living atlas web portal), Maxar and Nearmap also provide ready-to-use building footprint datasets.

With its vast and ever-expanding collection of geographic data, OSM is one of the world's biggest and most active open data suppliers. For instance, China's OSM building data increased 20 times between 2012 and 2017 (Tian, Zhou and Fu, 2019). Based on the completeness check done by Biljecki et al. (2021) of OSM data with respect to government open data in 28 countries, coverage of OSM had a 95% (ratio of buildings recorded in EUROSTAT to the number of buildings retrieved from OSM in February 2021). Established in 2004, OSM functions as a cooperative, crowd-sourced mapping platform where a global community of contributors actively engages in mapping the surface of the planet (OpenStreetMap, 2023). Since OSM data is publicly available and free to use, a wide range of people, including academics, developers, companies, and nonprofits, may access it. Within the geographic community, creativity and cooperation are encouraged by this open-access ideology.

As OSM coverage grows worldwide, several studies have examined the use of OSM data for BIM applications. Bagheri, Schmitt and Zhu (2019) conducted a comprehensive assessment of the feasibility of applying OSM building footprint data as source data to generate 3D models of buildings. They also highlighted that one of the major issues in OSM data is that building footprints are generated as a whole even though the building has multiple blocks of different heights; thus, a preprocessing step is necessary to split into multiple blocks. In a study conducted by Girindran et al. (2020) on the generation of 3D models from open data, they realised that 3D models could be generated by a fusion of OSM with DSM data. However, it is important to highlight that this study did not consider available topological errors in OSM data.

While OpenStreetMap (OSM) provides several benefits as a major open data source, it is critical to recognise specific limitations and concerns related to its use. These difficulties may influence OSM's appropriateness for various applications and environments. The quality of OSM data is one of the primary problems when utilising it. Because the majority of OSM data is contributed by non-professionals, both the coverage and the quality of the data are dubious (Haklay, 2010; Senaratne et al., 2016). Even though a sharp rise in OSM data is observed, the third dimension is very poorly represented in OSM data, specifically for building height (Masson et al., 2020; Bernard et al., 2022). According to Lao et al. (2018)- cited in Bernard et al. (2022), less than 3% of buildings worldwide have a height value, and less than 4% have a number-of-floor value. While OSM is an excellent resource, users should be aware of its limitations, which include potential data mistakes, inadequate coverage, reliance on volunteers, limited attribute information, and the need for ongoing maintenance. Therefore, when considering if OSM is the best data source for 3D building modelling, these criteria must be carefully considered.

The existing body of research often focuses on evaluating the quality of OSM data and assessing factors such as completeness, consistency, and positional accuracy. However, there appears to be a scarcity of studies specifically dedicated to proposing and testing methodologies to actively improve the accuracy of the data within the OSM platform, which marks a potential research gap in the literature. The work of Zhuo et al. (2018) is a significant contribution in this domain as it focuses on the optimisation of OSM footprints using UAV images. Their approach of using a deep learning neural network proved to produce a large offset in terms of quality when compared with original OSM building footprints.

Government open data websites throughout the European Union, including the Czech Republic, are useful sources of reliable building information. These portals often include a variety of geographic data, such as building footprints, which may be used for urban

planning, infrastructure construction, and a variety of research purposes. Czech national mapping agency called State Administration of Land Surveying and Cadastre (ČÚZK), with the launch of the national online portal, has had a major influence on the availability of geographical data. ČÚZK started offering direct access download services for RÚIAN data, including digital cadastral maps in the digital format, on January 1, 2014, on the basis of the unified Creative Commons CC BY 4.0 license (ČÚZK, 2023).

Hron and Halounová (2019) conducted a study on creating roof models from building footprints in the Czech Republic. In this study, they utilised building footprints published by the Land Survey Office (NMA) of the Czech Republic, which is responsible for managing the national GIS database. The authors conducted tests on a limited dataset comprising around 30 buildings with diverse characteristics, including different shapes (vertices ranging from 4 to 16) and varying roof complexities (roof types, which ranged from 1 to 3) and mentioned that excellent results demonstrated particularly for simple and moderately complex buildings.

2.5 Building height detection

The precise identification of building heights is a crucial component in 3D building modelling as it forms the basis for many important applications. Building heights must be precisely determined to guarantee that 3D models accurately depict the real buildings, which will support the decision-making process. Determining the heights of buildings becomes especially important in situations when vertical dimensions are critical to the overall sense of space. Building height detection has been done using a variety of methodologies over time, demonstrating the ongoing development of technology and data sources. The complexity and accuracy of building height identification have significantly increased with the improvements in these approaches, enabling more accurate and efficient results in many scenarios.

2.5.1 Definition of building height

The definition of building height varies across different studies and contexts, reflecting the nuanced considerations and objectives within each field and the application. According to American Legal Publishing (n.d.) In multifamily residential buildings built in compliance with unified residential development regulations, the height is determined by measuring from the top of the completed slab to the top of the tallest wall top plate (Figure 4). They further mentioned that in buildings other than multi-family homes, the height will be measured according to Figure 5.

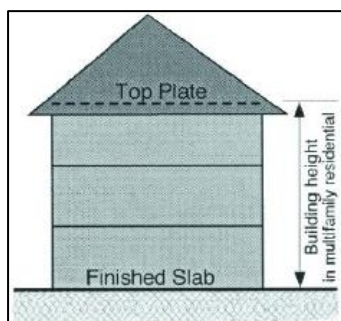


Figure 4: Height in multifamily residential (ALP, n.d.)

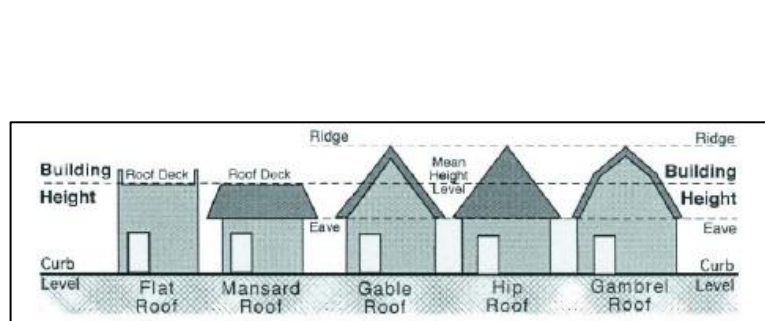


Figure 5: Measuring building height (ALP, n.d.)

2.6 Methods of building height detection

2.6.1 Deep learning

The advent of deep learning neural networks has significantly influenced the field of building height estimation, leading researchers to increasingly adopt these advanced techniques. As building structures react differently to multiple viewing angles, such as in terms of spectral and structural changes, multi-view satellite images can explain the vertical information of buildings. However, deep learning-based building height estimates have not made use of these images. As a novel approach, Cao and Huang (2021) introduced M3Net, which uses multi-view ZY-3 images with a spatial resolution of 2.5m to estimate building height. After testing the methodology in 42 Chinese metropolitan areas having diverse building types, the results indicated lower root mean square error than the random forest method and vanilla single/ multi-task models. The approach also verifies the scalability of the methodology further since the test was also done in a comparably broader region of extent. Another neural network-based approach implemented by Li, Chen and Lin (2022) shows that single images can be used to restore height information, unlike the method implemented by Cao and Huang (2021). Lin's (2022) approach consists of two main stages: 1. Rotation shadow detection, 2. Building height calculation. Their methodology stands out from the rest due to its simpler implementation, fewer sources of data, and greater accuracy.

2.6.2 Open data sources

One of the major issues in building height estimation is the unavailability of open data sources. To address this issue, in recent years, many researchers have focused on implementing methodologies to estimate height information from open data, such as Sentinel 1/2, for large-scale mapping applications. Since Koppel et al. (2017) found a strong correlation between height information and Sentinel 1 backscatter characteristics, a whole new realm of applications was introduced in large-scale 3D modelling. Li et al. (2020) used these correlation characteristics to implement a comprehensive methodology to estimate building height from Sentinel 1 data. First, they implemented a height indicator using dual-polarization (VV and VH) and generated a building height model from the indicator. The RMSE was 1.5 meters when comparing the outcomes with a lidar-based model; this value also outperformed the precision of the data released by Advanced Land Observing Satellite (ALOS) DSM (X. Li et al., 2020). Even though very high accuracy was obtained in terms of RMSE, Huang et al. (2022) mentioned that due to layout, high reflectivity from some metal materials, double-bounce scattering, and other factors, backscatter coefficients from Sentinel-1 data were not consistent in some areas. Cai et al. (2023) implemented a multi-spectral and Synthetic Aperture Radar (SAR) data fusion approach that utilises Sentinel 1 and 2 publicly available data. Their method employs a multi-modal selective kernel (MSK), which can reach an RMSE of less than 5m after testing it in 63 Chinese cities. Therefore, considering the RMSE of methodologies of Cai et al. (2023) and Li et al. (2020), using the dual-polarization method seems more accurate.

Huang et al. (2022) emphasised that there are two major issues even though the above methods from ALOS and Sentinel 1/2 data sources support the field of large-scale building height estimation: 1. Lacking considering the topographic environment, 2. Prior research mostly concentrated on predicting building height at coarse resolution; further work is required to estimate building height at fine resolution on a broad scale. Therefore,

the methodology implemented by Huang et al. (2022) is composed of utilising ALOS World 3D-30m (AW3D30) DSM and other supplementary data with a novel slope correction algorithm for height estimation.

Google Earth is a web-based geospatial application that gives users an interactive and thorough representation of the surface of the planet. With the use of aerial photography, satellite imaging, and GIS data, Google Earth provides a three-dimensional view of the world's cities, structures, and landscapes. In the context of building height estimation, Google Earth proves to be a valuable resource. The platform integrates 3D models to represent buildings and structures with realistic elevation data. Qi, Zhai and Dang (2016) implemented a comprehensive methodology to calculate building height using Google Earth. Their methodology utilises the shadow of the building to estimate building height using the length of the shadow and the terrain slope. In situations where the building shadow is not clearly visible, they proposed a new step which considers celestial geometry.

2.6.3 LiDAR data processing

Building height estimation has been transformed by Light Detection and Ranging (LiDAR) technology, which provides precise and comprehensive elevation data for a wide range of applications. LiDAR technology operates by sending laser pulses from an aerial or ground-based platform and measuring the time it takes for the laser to return after colliding with a surface (Wasser, 2023). This method enables LiDAR to produce very precise three-dimensional point clouds that capture the topography of the Earth's surface, including buildings and other structures.

Utilising LiDAR data for 3D applications has been around for more than two decades. One of the earliest studies was done by Morgan and Tempfli (2000), where they used a LiDAR dataset of 2-3 points per m² with Laplacian and Sobel operators to separate buildings from trees. Rottensteiner and Briese (2003) retrieved the building's top surface to create a polyhedron model, thereby calculating building height using region growth and curvature-based segmentation technologies from a DSM generated from LiDAR data. Erener, Sarp and Karaca (2020) used a data fusion approach that used aerial imageries and LiDAR data to estimate building height. In their study, Normalized Digital Surface Model (NDSM) was created considering the first and last return of the LiDAR dataset. The definition of building height is considered to be the maximum height value within the building footprint outline. Although the study displays the accuracy evaluation for the predicted number of floors in relation to ground truth, there is no accuracy assessment for the building height.

In order to calculate building height, some researchers utilised statistical approaches such as zonal statistics and normal distribution functions. Zhang, Han and Bogus (2020) conducted a study to extract building height and footprint extraction from LiDAR and Aerial imagery. In their study building height is considered as the mean of the NDSM covering the building footprint. They used zonal statistics calculation to determine the height of the building. However, when modelling 3D models of existing buildings, it is important to have actual height information of buildings, such as highest and lowest points rather than mean value.

Calculating building height by integrating LiDAR data with building footprints poses challenges, notably when ground pixels in the NDSM overlap with the footprint. This situation can lead to inaccuracies in roof values, introducing errors in metrics such as minimum and maximum roof heights. To address this issue, outliers resulting from these

discrepancies must be identified and removed to ensure the precision of the height estimation. A solution proposed by Hron and Halounová (2019) involves using the 95th percentile as the top height value within the footprint. Simultaneously, the roof bottom value is determined as the third percentile within a 1-meter radius both inside and outside the building footprint. By adopting this approach, the overall roof height is calculated as the difference between the top height and the bottom height, mitigating the impact of outliers and enhancing the reliability of the building height estimation process.

2.7 Roof modelling

Roof modelling stands as a pivotal facet in architectural and geospatial research, providing a comprehensive understanding of the built environment's intricate details. This process involves the digital representation of rooftops, capturing their diverse forms and features. Beyond mere visual aesthetics, Its applications, ranging from urban planning and energy efficiency to telecommunications and disaster management, highlight its significance as a multifaceted tool in enhancing our understanding of the built environment (Hron and Halounová, 2019).

Various studies have explored and proposed diverse methods for identifying the type of roof in roof modelling, leveraging advancements in technology and data analysis. One of the most common methodologies is to utilise slope and aspect calculations to identify the type of roof. In the GIS domain, the rate of change between each cell and its neighbours is estimated via raster-based slope computing algorithms, while the aspect refers to the compass direction that a slope faces (wiki.gis.com, n.d.). Gergelova et al. (2020) used these tools to identify different types of building roofs as an initial step for the reconstruction of roofs. The study used mean slope values of the roof to identify flat roofs and pitched roofs; thus, slope $\leq 10^\circ$ are flat roof buildings; in contrast, $10^\circ < \text{slope} < 45^\circ$ are pitched roof buildings. In their work, they considered six types of roofs, as mentioned in Figure 6.

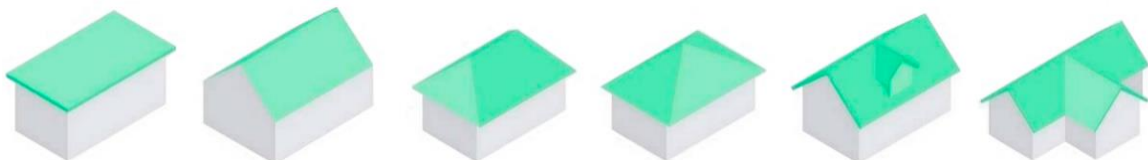


Figure 6: Types of roofs considered by Gergelova et al. (2020)

Another important step in roof modelling involves identifying the shape of the roof and roof planes. Many researchers used the flow direction algorithm- a method originally used for deriving the direction of the flow and the volume of the flow. The eight neighbouring cells that flow might enter have eight appropriate output directions associated with them, as mentioned in Figure 7. This method, sometimes called an eight-direction (D8) flow model, is based on a strategy that Jensen and Domingue (1988) introduced.

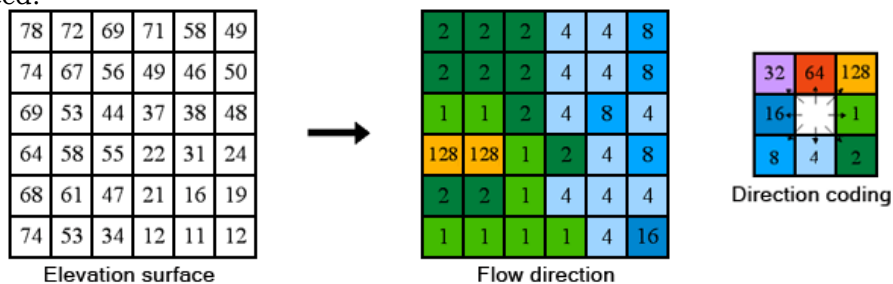


Figure 7: Flow direction D8 method by Jensen and Domingue (Esri, n.d.)

Gergelova et al. (2020) used this approach to identify the form of the roof ridge and determine the number of planes and their slope directions, thereby determining the type of roof. In the work of Hron and Halounová (2019), they used a line segment detector (LSD) algorithm which detects straight contours on grayscale images without tuning parameters. They claim that the edge detection technique, which is a component of the Open-Source Computer Vision Library (OpenCV), is incredibly fast and produces good results without the need to modify any parameters. They have also highlighted certain drawbacks of their approach, such as the current implementation does not allow modelling of roof ridges except in the middle or on the outline of buildings and obstacles resulting from assigning rules for individual roof types.

Random sample consensus (RANSAC) is another approach that multiple researchers used to extract roof planes (Tarsha-Kurdi, Landes and Grussenmeyer, 2007; Kleineberg, 2018; Gönültaş, Atik and Duran, 2020; Mohammadzadeh, 2020; Chen et al., 2021). According to Fischler and Bolles (1981) – the founders of the algorithm, RANSAC takes the least amount of information possible and then expands it with consistent data points in contrast to traditional sampling approaches that utilise as much data as feasible to generate an initial answer and then proceed to trim outliers. Multiple researchers have used the RANSAC algorithm to extract roof planes from LiDAR data. Mohammadzadeh (2020) applied the RANSAC algorithm to a LiDAR point cloud of a building dataset and determined the optimal plane through the candidate points that comprise the roof plane based on the geometric location of the points and distance to the plane. Kleineberg (2018) also used the RANSAC algorithm to detect roof planes, which is an initial step in generating 3D meshes of building roofs using a LiDAR point cloud. Later, he created a new algorithm to generate convex roofs in a unity engine. Therefore, considering the final results of Mohammadzadeh (2020) and Kleineberg (2018), it is evident that the RANSAC algorithm looks promising for finding roof planes, which is an initial step in generating 3D models of roof structures. However, according to Canaz Sevgen and Karsli (2020), the RANSAC algorithm has certain limitations in situations when some points are located within the roof plane which are not part of the roof plane. To mitigate this problem, they developed I-RANSAC, a modified algorithm that searches just points on the surface based on a specific threshold value, excluding outliers over the threshold value.

Clustering in roof modelling is a data analysis technique that involves grouping together roofs with similar characteristics, patterns, or attributes. This process is particularly valuable for identifying commonalities among roofs within a dataset, aiding in the classification, segmentation, and analysis of diverse roof types. Many researchers have utilised numerous clustering methodologies to identify roof planes (Sampath and Shan, 2008; Kong, Xu and Li, 2013; L. Li et al., 2020; Hong et al., 2021). One of the earliest studies that used clustering techniques for roof segmentation was done by Sampath and Shan (2008). They used eigenvalue and eigenvector analysis to determine locations that lie along the roof edges, i.e. along the links of multiple roof planes, and thereby create a 3D model of the roof. , and Li (2013) used a combined approach using two clustering methods: K-plane and K-means algorithms. In order to identify the initial cluster centres, they also implemented a new initialisation method that uses mathematical morphology and the Hough transform technique.

2.8 Software and built-in workflows for 3D modelling

3D modelling software plays a pivotal role in the field of architecture and building design, offering architects, engineers, and designers powerful tools to visualise, analyse, and communicate complex ideas. These software applications enable professionals to

create detailed 3D representations of buildings, facilitating a more comprehensive understanding of spatial relationships, aesthetics, and functional aspects.

Esri's ArcGIS Pro is a full-featured commercial desktop GIS program that allows users to explore, view, and analyse data, as well as compile 2D and 3D maps (Esri, n.d.b). Additionally, ArcGIS Pro provide step-by-step automated workflows with minimal user interaction for various application domains, including 3D modelling with LiDAR point cloud data. According to Esri (2023), 3D building solutions provide automated workflows for extracting normalised elevation surfaces, creating building footprints and subsequently generating 3D models, creating building floors and predicting the type of building roof. However, there has been little to no empirical proof of the workflow's performance for modelling 3D structures since it was initially announced in July 2023.

Esri CityEngine is another commercial urban planning and modelling software that enables the creation of realistic cityscapes. It streamlines the design process by generating detailed urban environments and enhancing spatial analysis for architects, urban planners, and GIS professionals. Oskoue, Babaei and Teymuri (2023) noted that the main aspect of modelling with Esri's CityEngine software is employing commands and rules, as well as scalability, to create large cities as easily as small cities without sacrificing quality. Since its inception, numerous researchers have extensively tested Esri CityEngine, affirming its prowess as a potent tool for city modelling (Edvardsson, 2013; Hu et al., 2013; Badwi, Ellaithy and Youssef, 2022). The software consistently demonstrates robust capabilities, earning recognition as an asset for researchers and professionals in urban planning and design. Badwi, Ellaithy and Youssef (2022) conducted a recent study with CityEngine, the main objective of which was to highlight the importance of 3D procedural modelling and its capabilities. They analysed and tested the CityEngine procedural modelling idea in Beni-Suef, Egypt, and concluded that CityEngine is a powerful 3D-GIS modelling program that creates realistic 3D models from 2D spatial data. However, it is important to emphasise that more complex scenarios should be investigated (Badwi, Ellaithy and Youssef, 2022). Another important highlight of Esri CityEngine is its capability to batch create 3D models (Esri, 2015). Unlike traditional modelling platforms, CityEngine is capable of creating reusable Computer Generated Architecture (CGA) scripts and integrating semantic rules (Hu et al., 2013). Also, Esri R&D Center Zurich (2010) created recommended CGA references and updated in 2014 to guide users to generate different building's roof types and incorporating different textures.

Trimble Inc.'s SketchUp is a flexible 3D modelling program that is extensively used in architecture, interior design, and other industries. SketchUp's user-friendly interface allows users to quickly generate and modify 3D models (Sketchup, n.d.). According to Singh, Jain and Mandla (2013), photogrammetry and laser scanning are common image-based approaches with limitations. To overcome these limitations, they proposed a simple, low-cost method for creating virtual 3D campuses for educational institutions. The model may be generated in a variety of formats, published on the web, and exported to Google Earth (Singh, Jain and Mandla, 2013). Sketchup also facilitates the automatic creation of models without primarily depending on manual push and pull methods. Since Sketchup supports Ruby programming language, users have the ability to automate workflows with minimal user interaction. Alizadehashrafi (2015) used Ruby language within Sketchup to generate windows and doors automatically. Ying, Li and Guo (2011) used a combination of software workflows such as ArcGIS and Sketchup to create a 3D cadastral system parameterising 2D survey plans. Ying, Li and Guo (2011) further

mentioned that as long as the original 2D set of polygons follows the Ruby criteria, the reconstruction could be made automatic.

Apart from the above software, numerous 3D modelling applications are available on the market. Autodesk Revit is a popular BIM program that includes 3D modelling, parametric modelling, collaborative capabilities, and documentation. It can handle complicated geometries and huge projects. Bentley Systems is also a popular BIM software which comes in editions including PowerDraft, Connect Edition, and V8i. Graphisoft ArchiCAD is renowned for its user-friendly interface, capacity to manage complicated projects, and other important capabilities, including parametric modelling, 3D modelling, documentation, and collaboration tools.

2.9 Accuracy assessment of 3D models

Accuracy assessment is an important aspect of 3D city and building modelling, playing a crucial role in ensuring the reliability and usefulness of these models. Assessing the accuracy of these models involves evaluating the fidelity of the representation of real-world structures and features. This process aids in identifying discrepancies between the virtual models and the actual physical environment. Sanz-Ablanedo et al. (2018), a fundamental way of assessing 3D model accuracy is by comparing the RMSE of Ground Control Points (GCP) or by measuring coordinates in the real world and the model. Unfortunately, this method can be used only for models created using photogrammetric methods. Therefore, it is evident that most of the accuracy assessment studies conducted for the models which were generated by photogrammetric methods.

When conducting an accuracy assessment of 3D models, it is important to characterise types of errors and their sources. Borkowski and Józków (2012) focused on this aspect and identified six sources of errors associated with 3D modelling: errors of Terrestrial and Aerial Laser Scanning (TLS and ALS), errors of integration of datasets, errors due to generalisation and topology correction and finally texturing errors. On the other hand, Michelin et al. (2013) highlighted three main sources of errors in 3D modelling: 1. footprint error- errors in building outline, 2. reconstruction errors- errors associated with algorithms and mathematical functions, 3. vegetation errors – when canopy covers the building and making difficult to model the 3D structure. However, Gabara and Sawicki (2021) argued that a new error category should be added to address problems associated with object complexity due to multi-part roofs, roof texture and type.

Over the years, many researchers introduced methods for the accuracy assessment of 3D models. Cheuk and Yuan (2009) implemented a simple method to evaluate the accuracy of generated 3D models according to a reference dataset. They transformed the referenced 3D building model into a grid structure, utilising the elevation attribute of building polygons. Subsequently, the building height grid was subtracted from the lidar data, and the resultant differences were categorised into five distinct classes. Borkowski and Józków (2012) also created multiple 3D models of buildings from different sources of data: ALS and TLS data, both representing identical locations. Subsequently, a comparative analysis was conducted to assess the errors inherent in the ALS and TLS datasets (Borkowski and Józków, 2012). Moreover, they proposed that the correctness of the models might be assessed by comparing the coordinates of the characteristic points in the models with the corresponding coordinates of these places on real structures. They gathered reference points on buildings using a Leica total station and compared them to matching model points. Gabara and Sawicki (2021) conducted a comprehensive analysis to compare the accuracy of the same 3D model from two different sources: 1. Polish

National Geoportal, 2. Trimble SketchUp Warehouse. They used the RIEGL point cloud as the reference dataset for assessing the quality and accuracy of 3D building models. This methodology provided a comprehensive analysis, combining visual insights from heat maps with quantitative metrics from histograms, to ensure a thorough assessment of the 3D building models' quality and accuracy against the reference RIEGL point cloud.

3 METHODOLOGY

In this chapter, the important stages of the research methodology will be presented briefly. Additionally, the tools and software utilised for gathering, analysing, and interpreting data will be outlined. Subsequently, an abstract representation of the overall methodology will be provided, offering readers a comprehensive overview. Finally, the six main stages of the methodology will be further explained, highlighting the purpose and significance of each.

3.1 Data and software used

To achieve the research goals, a variety of software tools and data sources have been used to facilitate data collection, analysis, and visualisation. These resources are essential to our methodology's resilience and effectiveness.

3.1.1 Data Sources

- **LiDAR data**

LiDAR data has been used as the major data source due to its ability to acquire extremely detailed and precise elevation data. LiDAR data gives exact three-dimensional reconstructions of the Earth's surface, making it possible to identify topographical features, land cover characteristics, and urban buildings with unprecedented accuracy. The data was created as part of the MOSPREMA project <https://mosprema.upol.cz/>. It consists of data from aerial laser scanning conducted by Primis company. The data was created in 03/2023 with a point density of 20 points per square meter of the last return.

- **Ortho imagery**

These high-resolution aerial images offer detailed visual representations of the Earth's surface, providing valuable context and spatial information for the analysis. The imagery sourced from the ČÚZK Geoportal is renowned for its quality and reliability, making it an indispensable asset in our research. However, a high degree of parallax error is observed in certain cases.

- **Building footprints**

Building footprint data offers critical information on the geographical distribution and features of developed buildings in the research area. It is also the key data utilised to calculate LOD2 buildings in research locations. The datasets were also collected from the ČÚZK Geoportal.

3.1.2 Software and programming languages

- **ArcGIS Pro**

ArcGIS Pro, a sophisticated GIS platform built by Esri, is the foundation of our spatial analytic methodology. ArcGIS Pro's advanced geoprocessing capabilities and intuitive interface make it easy to integrate, visualise, and analyse a wide range of spatial information, such as LiDAR point clouds, orthoimages, and building footprints.

- **Esri CityEngine**

Esri CityEngine allows for the production and study of detailed 3D urban models. CityEngine uses procedural modelling approaches with CGA to generate accurate representations of urban landscapes, including buildings, topography data, and vegetation layers. This software tool allows us to model urban development scenarios and evaluate the spatial effect of planning initiatives.

- **Python**

Python is a popular programming language within the scientific community. In the study, multiple Python packages were used for accuracy assessment and visualisation (Matplotlib, Pandas, Scikit-learn and mplotcursors). Matplotlib is a sophisticated Python charting package. It supports a broad range of customisable plots and charts, such as line plots, scatter plots, bar charts, histograms, and others. mplotcursors is a Python module that improves the interactivity of Matplotlib graphs by including cursor annotations. It lets users see further details about points of data when they hover over them with the cursor. Scikit-learn is a Python machine-learning package that provides easy-to-use data mining and analysis capabilities. In this study, it was utilised to assess the accuracy of parameter calculations.

3.2 Abstract representation of the methodology

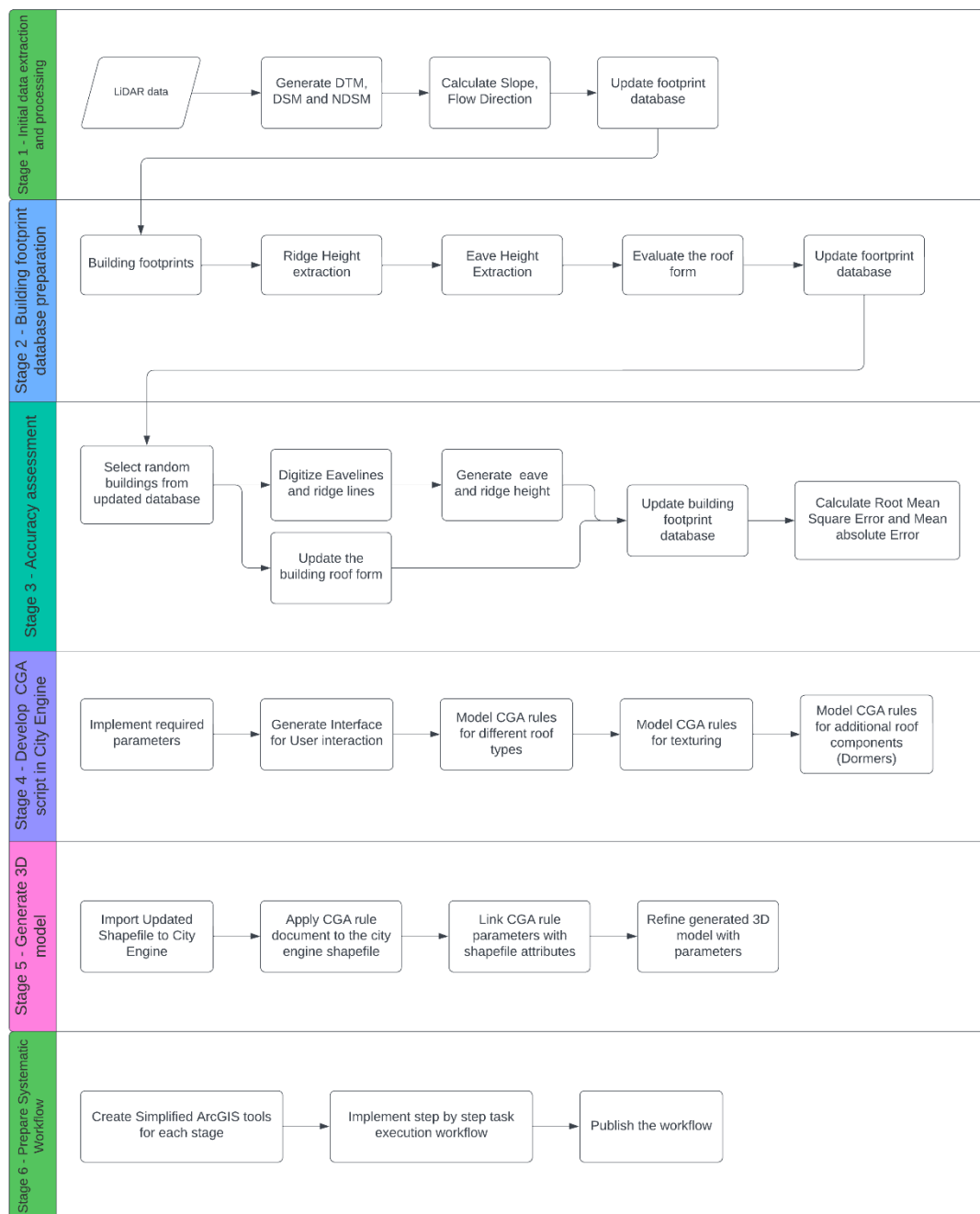


Figure 8: Abstract methodology

3.2.1 Stage 1 – Initial data extraction and data processing

- **Generate elevation surfaces (DTM, DSM and NDSM)**

Esri published a workflow to automate the generation of 3D multi-patch buildings (Esri, 2023). Although the final output could be more accurate, one of the steps involves running a Python-based script within ArcGIS to extract the above-mentioned elevation surfaces by processing .las files, which is the most common LiDAR data storage format. This study uses this script to extract elevation surfaces for further processing. These surfaces provide valuable insights into the topography of the study area, the distribution of above-ground features, and the morphology of buildings and structures.

- **Generate slope and slope direction of each building.**



The Building Slope Analysis Model, created using Model Builder in Esri ArcGIS Pro, is designed to assess the slope of building structures based on high-resolution elevation data. The model comprises four primary steps: create a 2m Buffer for building, extract NDSM raster by mask, fill voids, generate flow direction, and evaluate slope.

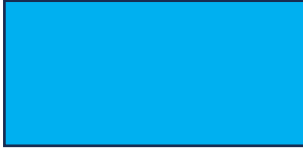
3.2.2 Stage 2 - Building footprint database preparation

- **Calculate eave height, ridge height and roof slope.**

Another critical stage of 3D building modelling involves extracting roof parameters such as ridge height, eave height, and roof slope. The model employs the “Zonal Statistics as a Table” as the primary tool to generate the above parameters. Instead of relying on traditional mean calculations which may be susceptible to outliers, the model adopts a more robust approach by evaluating percentile values and median using the Zonal Statistics as Table tool. This methodology ensures that extreme values do not unduly influence the analysis, resulting in more reliable and representative results. After calculating these parameters, the values will automatically update the attribute table of the building footprint feature layer. Table 1 shows the configuration used to calculate the above parameters.

Table 1: Statistical values and methods for calculating the above parameters

Parameter	Method	Statistical value
Eave height	<p>1 – Consider NDSM heights 0.25m on either side of the building boundary</p>  <p>2 – Consider NDSM heights within a 0.5m inward buffer from the building's edge.</p> 	50 th percentile, median, 90 th and 95 th percentile

Ridge height	Consider the entire building footprint when evaluating with NDSM and slope raster. 	Median, 75 th , 90 th and 95 th percentile for ridge height.
Roof slope		Median, mean, 90 th and 95 th percentile

- **Evaluate the roof form**

Classifying roof types is a crucial aspect of 3D building modelling. The methodology outlined below presents a systematic approach to classify roof types, incorporating both slope characteristics and directional analysis of roof structures.

Step 1: Identification of sloped and flat roofs

Ridge height and eave height difference: The first step involves distinguishing between sloped and flat roofs. This is primarily achieved by evaluating the difference in elevation between the ridge height and the eave height of buildings. A significant disparity between these two heights typically indicates a sloped roof structure.

Slope calculation: Additionally, mean slope calculations are employed to further differentiate between sloped and flat roofs. Higher mean slope values correspond to sloped roof structures, while lower values suggest flat or nearly flat roofs.

Step 2: Classification of different pitched roofs:

After identifying sloped roofs, the next step focuses on classifying different pitched roof types, such as Shed, Gable, and Hip roofs. This classification is achieved by analysing the distribution of roof pixels in eight different directions relative to the building footprint by conducting flow direction analysis and calculating overall pixel percentages in each direction.

3.2.3 Stage 3 – Accuracy assessment

Step 1 – Select a set of random buildings from the study area.

This step randomly selects a representative set of buildings from the study area. This selection aims to ensure a diverse sample that adequately represents the variability of building structures within the study area. This step is done automatically by running a Python script within a model builder code block.

Step 2 – Digitize and generate eave lines and ridge lines of the selected buildings.

Once the random buildings are identified, their respective eave lines (the lower edge of the roof where it meets the walls) and ridge lines (the highest point of the roof) are manually digitised from available building footprints or point cloud data. The digitisation process ensures an accurate representation of the roof geometry, enabling precise calculations of ridge height and eave height for accuracy assessment.

Step 3 – Update roof forms based on ortho imageries.

After digitising the eave and ridge lines, a new field is added to update the roof forms based on the ortho imageries. This step helps validate and adjust the accuracy of the initially detected roof forms by comparing them with visual evidence from the imagery. Any discrepancies or inaccuracies between the detected roof forms and the Ortho imagery are identified and corrected, ensuring the reliability of subsequent analyses.

Step 4 – Calculate error statistics.

Error statistics are calculated to quantify the accuracy of the ridge height and eave height calculations, as well as the automatic detection of roof forms. Common error metrics include:

Mean Absolute Error (MAE): The average absolute difference between the detected and ground-truth ridge heights and eave heights. Lower MAE values indicate higher accuracy.

Root Mean Square Error (RMSE): The square root of the average of the squared differences between the detected and ground-truth heights. RMSE measures the overall deviation between the predicted and actual values.

Confusion matrix: The proportion of buildings for which the automatically detected roof forms match the updated forms based on ortho-imagery.

These error statistics provide insights into the precision and reliability of the ridge height and eave height calculations, as well as the effectiveness of the automated roof form detection algorithm.

3.2.4 Stage 4 – Develop CGA script in Esri CityEngine

- **Modelling basic roof types**

Esri CityEngine provides CGA syntax for four main types of roofs (Hip, Gable, Shed and Pyramid) in addition to flat roofs (Figure 9). This syntax can be adopted to generate several other roof types, as explained in the Esri CityEngine tutorial series.

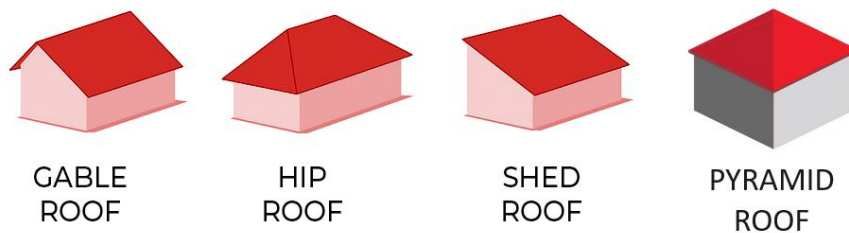


Figure 9: Basic types of roofs that can be generated

- **Modelling complex roof types**

In addition to the five basic roof types, including flat roofs, ten additional roof types are implemented. Figure 10 visualises each of the ten roof types, illustrating their distinctive shapes and architectural characteristics.

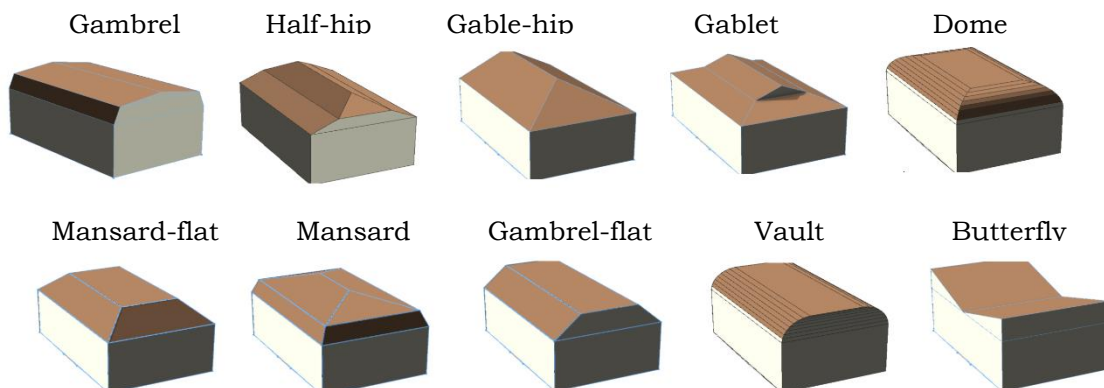


Figure 10: Complex building roof types considered

- **Implement a Graphical User Interface (GUI) for user interaction**

A user interface is implemented to allow users to interactively manipulate 33 parameters related to the 3D building modelling. These parameters encompass various aspects of the 3D modelling process, including visualisation options, building attributes, roof-related attributes, single-dormer attributes, and double-dormer attributes.

- **Modelling CGA rules for texturing**

Two distinct methods of visualising roofs and facades are implemented: realistic visualisation and solid colour representation. Realistic visualisation utilises textures imported from the Esri CityEngine built-in library. These textures enable intricate detailing and lifelike rendering of roofs and facades, enhancing the visual appeal and realism of the models; however, these textures do not correspond to the actual appearance of the models. Conversely, solid colours provide a simplistic yet customisable approach, allowing users to interactively adjust colours according to their preferences and requirements.

3.2.5 Stage 5 – Generate 3D model

Stage 5 of the methodology for generating 3D models using Esri CityEngine begins with importing essential geospatial data, including shapefiles detailing building footprints, DEMs capturing terrain elevations, and orthophotos providing aerial imagery. This data forms the foundational framework for subsequent modelling steps. Next, the imported shapefiles are aligned with the terrain to ensure spatial accuracy, facilitating proper placement of building structures atop the terrain surface according to the DEM. Later, according to Figure 11, CGA rule parameters are linked with shapefile attributes, automating 3D building model generation based on predefined rules and attribute values. This linkage enhances adaptability and responsiveness to building attribute variations. Furthermore, the generated 3D models are refined using additional parameters to enhance realism and accuracy, including adjustments to building heights, roof styles, facade textures, and architectural details like dormers. Through these systematic steps, the methodology aims to create accurate and visually compelling representations of the built environment.

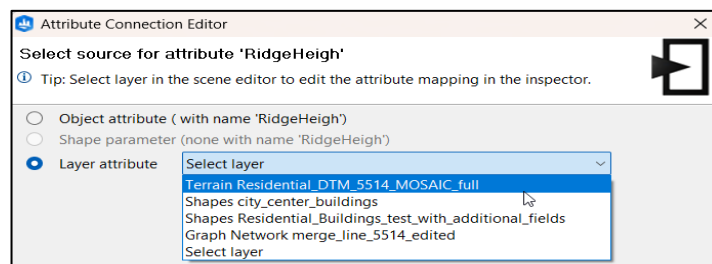


Figure 11: Parameters - attribute linking

3.2.6 Stage 6- Prepare systematic workflow

ArcGIS Pro allows users to create tasks, giving users a streamlined and easy approach to automate workflows and execute repetitive activities quickly. According to Esri (n.d.), a task is a preset series of steps to lead users through a workflow or business process. Thus, it may be used to create interactive tutorials, increase workflow efficiency, or help apply best practices. This study used ArcGIS Pro task implementation to create a systematic pipeline so users could easily execute the steps accordingly.

4 ROOF PARAMETERS CALCULATION

4.1 Initial data processing

Initial data processing consists of four main steps, each essential for preparing geospatial data for analysis. These steps include creating a 2-meter buffer around building footprints, extracting NDSM raster data within the buffered area, filling voids within the NDSM raster, and generating flow direction while evaluating slope. To streamline the entire workflow, the model represented by Figure 12 was implemented.

1. **Create a 2m Buffer for Building:** In this step, a 2-meter buffer zone is generated surrounding the outlines of building footprints. This buffer defines the area of interest for subsequent analysis, with a specific focus on the surroundings of the buildings. The buffer is used as the foundation for further processing and analysis, ensuring that the relevant geographic features are encompassed within the designated zone. Creating a buffer is critical to identify if the roof structure is expanded beyond the boundaries of the initial building footprints.
2. **Extract NDSM Raster by Mask:** The buffer created in the previous step serves as a clipping mask for extracting the NDSM raster data corresponding to the defined area of interest. The NDSM provides crucial elevation information relative to ground level, which is essential for conducting detailed slope analysis. By isolating the NDSM data within the buffered area, a focus is placed solely on the terrain surrounding the buildings, enabling meaningful insights to be derived. This step ensures fast execution in later steps since it only focuses on specific regions.
3. **Fill Voids:** Any voids or missing data within the NDSM raster are addressed to ensure the completeness and accuracy of the dataset. Voids or missing data can arise due to various factors, such as data acquisition errors or inconsistencies. This step is critical when conducting flow direction analysis in the next step.
4. **Generate Flow direction and evaluate slope:** The final step involves computing the flow direction based on the filled NDSM raster and evaluating the slope of the building surfaces using specialised tools such as the Surface Parameter tool. Valuable insights into the steepness or gradient of the building's terrain are obtained by analysing the flow direction and slope, which will be utilised during roof classification.

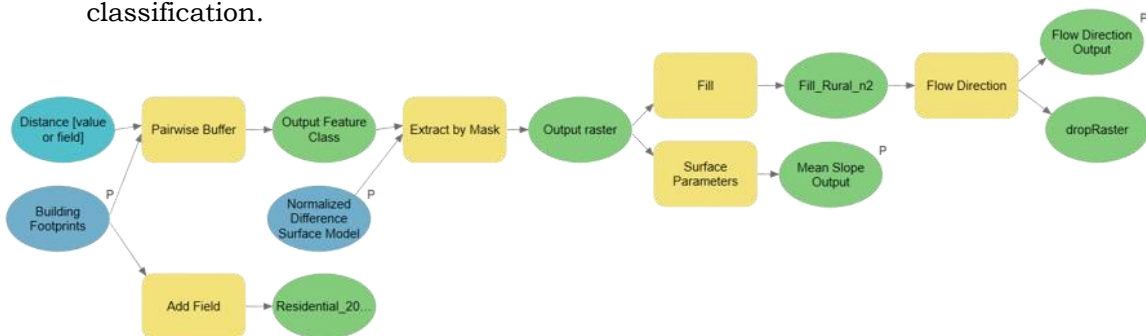


Figure 12: Model generated for extracting initial data

In the initial data processing phase of 3D modelling, one crucial step involves addressing building footprints that exhibit multiple roof types. This scenario often arises in urban environments where structures composed with heterogeneous roof designs within a single footprint. To ensure accuracy and fidelity to the original structures, it is

important to split these complex footprints into distinct components, each representing a unique roof type that is supported by the system.

4.2 Slope, ridge and eave height calculation

4.2.1 Evaluation of roof slope

In the calculation of slope, the Zonal Statistics tool of ArcGIS Pro was utilised, with the building slope raster generated in the previous step serving as the input raster dataset. Building footprints were employed as the zone layer parameter for the Zonal Statistics tool, defining them as the zones for which slope statistics were to be computed. This approach allowed for the aggregation of slope values within each building footprint, providing insights into the overall characteristics of the building roof.

Following the execution of the Zonal Statistics tool, statistics such as median, mean, 90th percentile and 95th percentile slope values were computed for each building footprint. To enhance the interpretability of the output, alterations were made to the field names associated with these statistics within the attribute table, ensuring clarity and consistency. Subsequently, the modified field names were joined back to the building footprints as new fields in the attribute table, facilitating further analysis and visualisation of the calculated slope parameters alongside other pertinent attributes of the buildings. Figure 13 shows the sub-process of the model that is used to automate the above workflow.

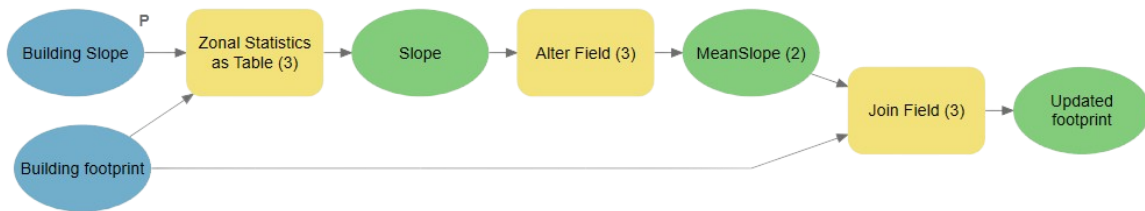


Figure 13: Calculation of slope of each roof

4.2.2 Evaluation of ridge height

A similar process was conducted for the calculation of ridge height. Instead of using the building slope raster, NDSM was utilised as the input raster dataset. The NDSM provides elevation information relative to ground level, which is essential for analysing ridge heights. Building footprints were again employed as the zone layer parameter for the Zonal Statistics tool, delineating the areas for which ridge height statistics were to be computed. This approach facilitated the aggregation of elevation values within each building footprint, allowing for the determination of ridge heights across the study area. Figure 14 represents a crucial part of the process, depicting a visual representation or diagram illustrating the steps involved in calculating ridge heights.

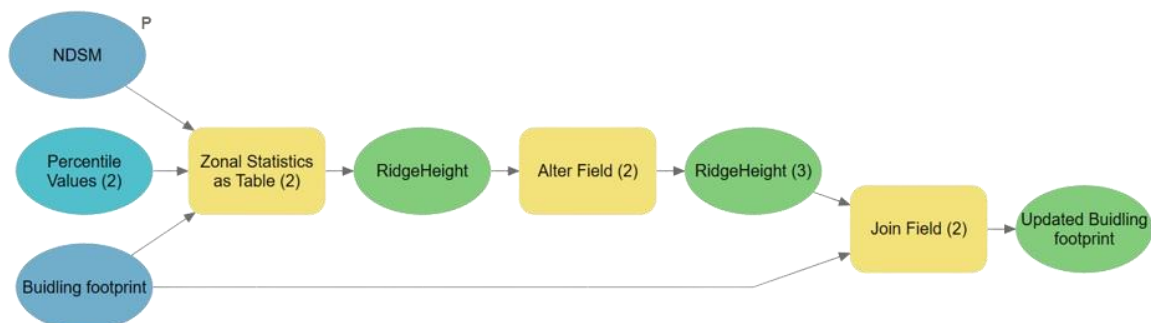


Figure 14: Calculation of ridge height of each roof

Upon executing the Zonal Statistics tool, statistics such as median, 75th percentile, 90th percentile, and 95th percentile ridge height values were computed for each building footprint. These statistics provide a comprehensive understanding of the variation in ridge heights across the landscape. During the accuracy assessment stage, the most suitable indicator among these statistics was selected, ensuring the reliability and relevance of the ridge height measurements for subsequent steps.

4.2.3 Evaluation of eave height

- **Method 1**

For the calculation of eave height, the building footprints were converted to polylines to facilitate further spatial analysis. Subsequently, a buffer of 0.5 meters was created around each polyline. This buffer delineated an area around the roof, focusing specifically on the eave region. The Zonal Statistics tool was then employed to compute relevant statistics for eave height estimation. In this case, the NDSM was used as the input raster dataset, providing elevation information relative to ground level. However, to ensure that only the eave region was considered for analysis, the zones for the Zonal Statistics tool were defined as the buffer features around the boundary of each building footprint.

Multiple statistical approaches, including the 50th percentile, median, 90th percentile, and 95th percentile, were utilised to capture the variability in eave height across the study area. Incorporating these statistical values helped to determine which method was more responsive to outliers. Figure 15 demonstrates the generated model to automate the steps.

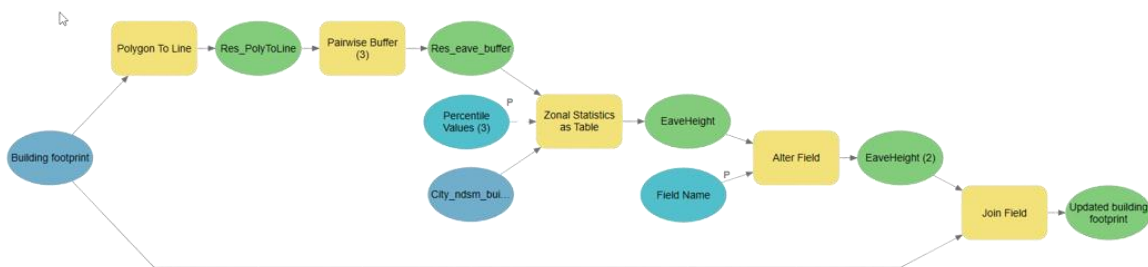


Figure 15: Eave height evaluation model (method 1)

- **Method 2**

For the second method, a distinct approach was adopted. Initially, a negative buffer of 0.5 meters was created around each building's footprint. This negative buffer delineated a portion surrounding the eave area inside the footprint. Subsequently, the Pairwise Erase tool was utilised to extract the difference between the original footprint and the negative buffer. This process resulted in the generation of a refined area corresponding to the eave region inside each building footprint. Following this step, the Zonal Statistics tool was employed once again. Accordingly, different statistical units, including median, mean, 90th percentile, and 95th percentile, were utilised to compute relevant statistics for eave height estimation. Figure 16 represents the entire workflow implemented to automate the process.

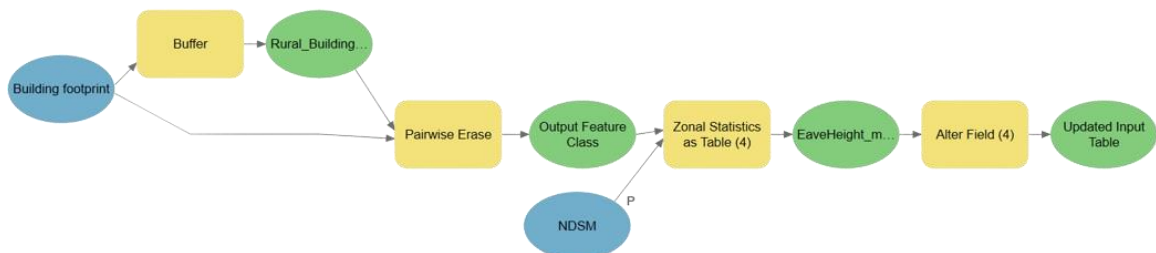


Figure 16: Eave height evaluation model (method 2)

4.3 Percentage of pixels in each direction

To assess the percentage of pixels covering the building footprint in each direction, the model represented in Figure 17 was implemented. Initially, the Tabulate Area tool was utilised to determine the extent of pixels covering the roof in each direction. This step provided valuable insights into the spatial distribution of pixel coverage across the building footprint. Following the determination of pixel extents in each direction, the total area was calculated by summing the extents in all directions using the Calculate Field tool. This cumulative total represented the overall area covered by pixels on the roof, serving as a reference for normalisation.

To facilitate comparison and analysis, it was essential to normalise these values. This was achieved by calculating the percentage of pixels in each direction relative to the total area. Each direction's extent was divided by the total area and multiplied by 100 to express the coverage as a percentage. This normalisation process ensured that all values were brought to a common reference, enabling the creation of common classification rules.

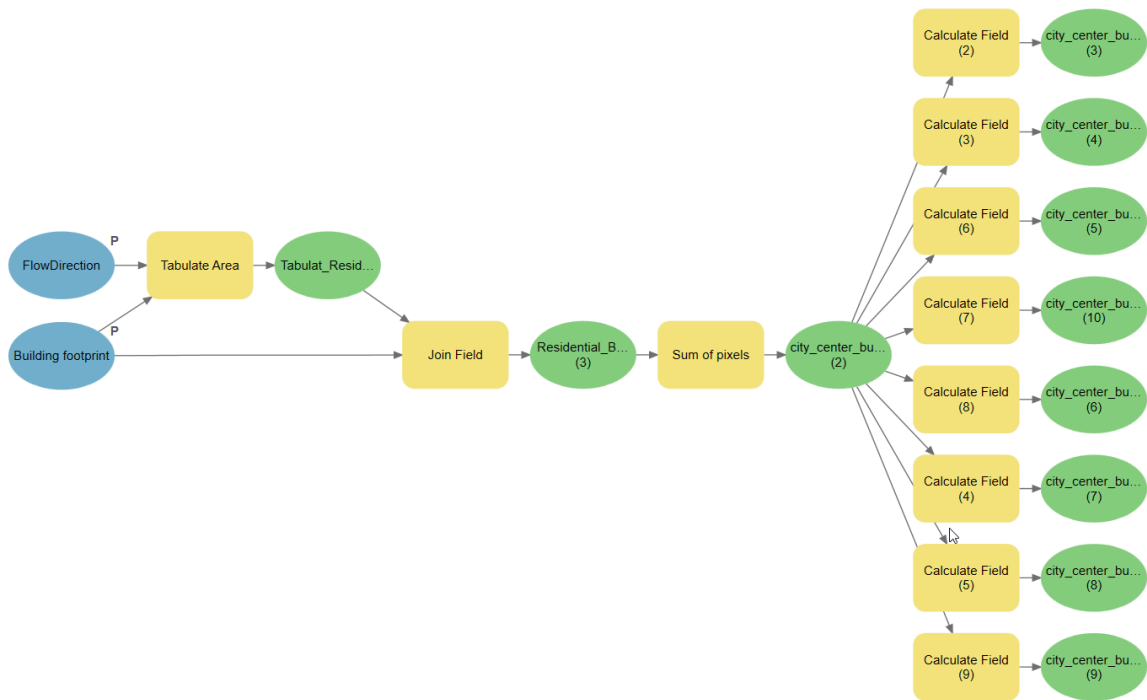


Figure 17: Roof direction extent calculation

5 CLASSIFICATION OF ROOF TYPES

Roof type categorization is an important stage in the 3D modelling workflow since it allows for proper representation of LOD2 models. This section provides a full explanation of the processes for automatically recognising various roof types.

5.1 Classification of flat roofs and pitched roofs

The classification of roofs into pitched and flat categories relied on a key indicator: the slope of the building. This methodological approach aimed to discern the structural characteristics of roofs within diverse geographic regions (residential, rural and city centre). Initially, data collection involved importing Excel files containing comprehensive building information for each study area. These files served as the foundation for subsequent analysis and have information such as the slope of the roof calculated using different methods, roof area, percentage of pixels in eight different directions, and the actual status of the roof, whether it is pitched or flat.

The most important step was to find the most suitable indicator for slope calculation. Accordingly, four statistical methods were utilised (95th percentile, 90th percentile, median and mean). To quantify and decide the most effective statistical method, an accuracy score was calculated to assess the classification's performance. It measures the ratio of correctly classified roofs to the total number of roofs. By plotting evaluation metrics against varying thresholds for each study area, the graphical representation facilitated a comprehensive understanding of the classification accuracy across different thresholds and select the best indicator.

According to Figure 18, it is evident that Mean (around 24°) and Median (around 15°) statistical indicators provide the best separation for pitched and flat roofs for all study areas. However, the Median give slightly more accuracy with respect to the mean (Table 2).

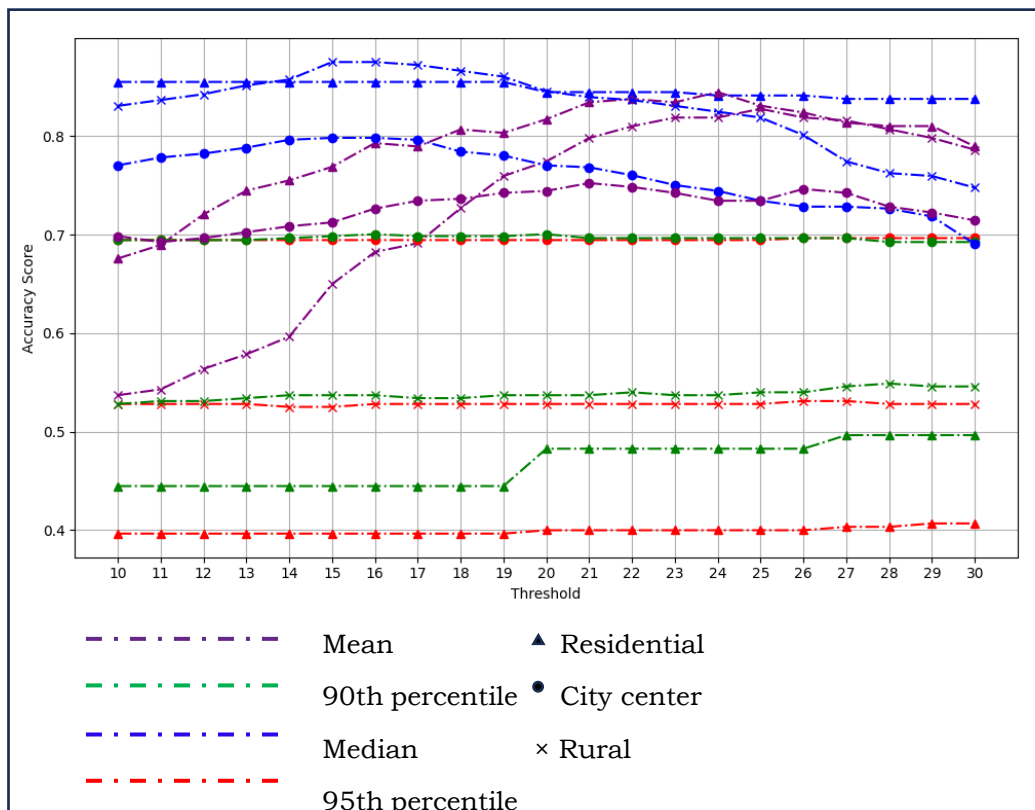


Figure 18: Accuracy vs roof threshold for different indicators

Table 2: Accuracy score of mean and median

Study area	Indicator	Threshold	Accuracy score
Residential	Median	<15°	0.8552
	Mean	<24°	0.8448
Rural	Median	<15°	0.8754
	Mean	<24°	0.8190
City centre	Median	<15°	0.7984
	Mean	<24°	0.7345

5.2 Classification of pitched roof types

According to Figure 19, certain roof types can be distinguished by the distribution of pixel percentages. This differentiation was achieved by analysing the directional pixel percentages derived from multiple radial graphs for each type of roof.

Flow Direction Analysis: The directions for analysis are obtained through flow direction analysis, which delineates the flow path of surface water runoff (Esri, n.d). This directional raster is utilised to determine the number of dominant directions, which is an indication of the number of roof directions.

Percentage Calculation: For each direction, the proportion of roof pixels in the associated segment is determined. This research sheds light on the prevailing orientation of the roof surface and aids in the classification of pitched roof types based on their various shapes and configurations.

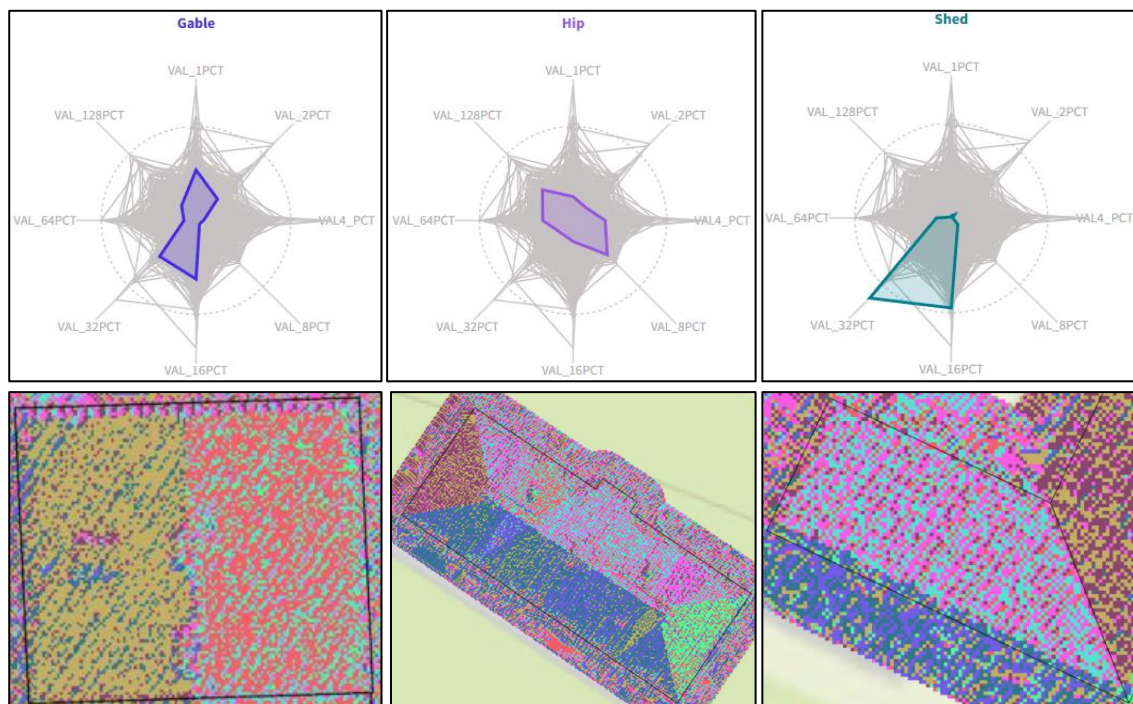


Figure 19: Distribution of pixel percentages of certain sample roof types

Gable roofs predominantly exhibited pixel percentages in opposite directions, while Shed roofs predominantly accounted for pixel percentages in a single direction. This observation was made by analysing radial graphs generated for each type of roof. After identifying these relationships between roofs, a Python code was used to model this relationship.

The code (Figure 20) utilised a function called `check_roof` to classify the roof types based on specific criteria. For instance, the function categorised roofs as Shed, Gable, or Hip based on the directional pixel percentages and other factors such as the sum of pixel percentages and the presence of pixel percentages in opposite directions.

```
def check_roof(row):
    if row['roof_status'] == 'Pitched':
        nums = [row['VAL_1PCT'], row['VAL_2PCT'], row['VAL4_PCT'], row['VAL_8PCT'], row['VAL_16PCT'],
                row['VAL_32PCT'], row['VAL_64PCT'], row['VAL_128PCT'], row['VAL_1PCT'], row['VAL_2PCT']]
        nums_sum = sum(nums[:3]) # Initialize sum for first 3 consecutive numbers
        for i in range(len(nums) - 2): # Iterate through the array
            if nums_sum >= 60: # Check if sum is greater than or equal to 60
                return "Shed"
            nums_sum -= nums[i] # Remove the first number from the sum
            nums_sum += nums[(i + 3) % len(nums)] # Add the next number to the sum
        # Get the values from the row
        values = [row['VAL_1PCT'], row['VAL_2PCT'], row['VAL4_PCT'], row['VAL_8PCT'], row['VAL_16PCT'],
                  row['VAL_32PCT'], row['VAL_64PCT'], row['VAL_128PCT']]
        std_deviation = pd.Series(values).std()

        # Check if there are two sets of two values in opposite directions
        opposite_pairs = [(0, 4), (1, 5), (2, 6), (3, 7)] # Pairs of indices corresponding to opposite directions
        pair_count = 0
        pair_count1 = 0

        for pair in opposite_pairs:
            if pair[0] in top_four_indices and pair[1] in top_four_indices:
                pair_count += 1

        for pair1 in opposite_pairs:
            if pair1[0] in last_two_indices and pair1[1] in last_two_indices:
                pair_count1 += 1

        # Check if both conditions are satisfied
        if sum_top_four >= 60 and pair_count >= 2:
            return "Gable"
        elif sum_top_two >= 40 and pair_count >= 1:
            return "Gable"
        elif sum_last_two <= 15 and pair_count1 <= 2:
            return "Gable"
        else:
            return "Hip"
    else:
        return "Flat"
```

Figure 20: Python function to classify roof types

This function takes a row of data as input, typically representing a single roof, and returns the classified roof type. This conditional statement checks if the roof status is 'Pitched'. If it is, the function proceeds with further analysis; otherwise, it categorises the roof as 'Flat'. Within the loop, if the sum of the three percentages' consecutive direction exceeds or equals 60, the roof type is classified as 'Shed'. This threshold value is based on observations from the majority of the shed roof types.

After analysing for Shed roofs, the function proceeds to analyse for Gable and Hip roofs based on additional criteria. This includes checking for pairs of percentages in opposite directions and sum thresholds. In this stage, the program takes the top 4 percentages and checks if these are in opposite directions. Accordingly, if there are two opposite pairs in the top 4 directions and the sum of the top is over 60, then that roof is classified as Gable. In the second condition for Gable, the top 2 percentages are considered, and if its sum is greater than 40 and is also an opposite pair, it is classified as Gable. As per the last condition, the program checks that the lowest percentages are less than 15 and are pairs.

6 GENERATE CGA SCRIPT AND LOD2 MODEL

6.1 Modelling roof types

6.1.1 Basic roof types

The implementation of different roof types, namely shed, gable, hip, and pyramid roofs, based on the CityEngine CGA rules, is integral to the generation of the LOD2 model. Figure 21 demonstrates a part of the CGA script that is used to implement the following basic types.

Shed Roof: defined in the CGA rules as 'roofShed'. It is characterised by a single sloping surface with an adjustable angle parameter. The 'RoofExtentReform' operation is applied to refine the roof extent and height, providing additional control over its appearance and alignment.

Gable Roof: represented by 'roofGable' in the CGA rules, features two sloping surfaces meeting at a ridge. Key parameters include the angle of the roof slopes, overhang dimensions, and the option to change the orientation of the ridge using the index argument. The 'RoofExtentReform' operation is again utilised to fine-tune the roof extent, ensuring optimal integration with the building geometry.

Hip Roof: in contrast to the gable roof, the hip roof, defined as 'roofHip' in the CGA rules, features multiple sloping surfaces converging to form the ridge. The angle parameter dictates the slope of each surface, with uniformity contributing to the characteristic appearance of the hip roof.

Pyramid Roof: implemented as 'roofPyramid' in the CGA rules, is characterised by multiple sloping surfaces with the same angle converging to form a point at the top. Like the hip roof, the angle parameter governs the slope of the roof surface.

```
# basic roof types
ShedRoof(Index) -->
    roofShed(15, Index) RoofExtentReform # 15 - angle but angle readjusted based on roof height

GableRoof(Index) -->
    roofGable(45, 0, 0, false, Index) RoofExtentReform
    print("scope.sy "+scope.sy)
    print("scope.sz "+scope.sz)
    /*angle, overhangX, overhangY, Make the roof gable even or not,
    Edge Index to control the orientation */

HipRoof -->
    roofHip(45) RoofExtentReform

PyramidRoof -->
    roofPyramid(45) RoofExtentReform
```

Figure 21: Implementation of basic roof types with CGA rules

6.1.2 Complex roof types

In CGA modelling, the implementation of complex roof types involves the combination of primitive roof structures defined above. Figure 22 and the following descriptions explore the methodology behind implementing different roof types using CGA rules, showcasing the flexibility of this approach in creating complex roof types using CGA.

Gambrel roof- starts with a gable roof of a specified angle. It then splits the roof vertically and applies a mass to the lower part while invoking a gable roof on the upper part at a different angle.

Half-hip roof- starts with a gable roof of specified angles and sets its height accordingly. It then splits the roof vertically and applies a mass to the lower part while invoking a hip roof on the upper part.

Gable-hip roof- combines elements of both gable and hip roofs. It is implemented by creating an envelope with a normal direction and specifying different components for the sides and front of the roof. While one side of the roof is normal to the eave, the other side has a specific angle, which corresponds to a hip roof.

Gable roof- like the Half-hip roof, this begins with a hip roof and splits it vertically. It sets the height of the upper part and applies a gable roof to it.

Mansard roof- The roof begins with a hip roof and splits it vertically. It sets the height of the upper part and applies a hip roof to it, creating the characteristic double-sloped profile of a Mansard roof.

Gambrel-flat and mansard-flat roof- types start with a gable roof and a hip roof, respectively. Later, a flat top is placed over both roof forms.

Vault and dome roof- structures rely on a recursive design pattern. Vault roofs utilise a series of gable roofs. In contrast, dome roofs employ stacked hip roofs to form a spherical shape.

```
GambrelRoof -->
  roofGable(70,0,0,false,Index)
  split(y){ Roof_Ht1*0.7: RoofMass(true)
            comp(f){ bottom: NIL | horizontal: set(Roof_Ht1,Roof_Ht1*0.3) GableRoof(Index) } }

HalfHipRoof -->
  roofGable(45,0,0,false,Index) s('1,Roof_Ht1,'1)
  split(y){ '0.5: RoofMass(true)
            comp(f){ bottom: NIL | horizontal: set(Roof_Ht1,Roof_Ht1*0.5) GableHipRoof(Index) } }

GableHipRoof(direction)-->
  envelope(normal,1000,comp(fe){all:0},comp(fe){direction:30|direction+2:90|all:30})
  comp(f){ all: RoofPlane }

MansardRoof -->
  roofHip(70)
  split(y){ Roof_Ht1*0.7: RoofMass(true)
            comp(f){ bottom: NIL | horizontal: set(Roof_Ht1,Roof_Ht1*0.6) HipRoof } }

GambrelFlatRoof -->
  roofGable(45,0,0,false,Index)
  split(y){ Roof_Ht1: RoofMass(false) }

MansardFlatRoof -->
  roofHip(45)
  split(y){ Roof_Ht1: RoofMass(false) }

GableRoof -->
  roofHip(45) s('1,Roof_Ht1,'1)
  split(y){ '0.5: RoofMass(true)
            comp(f){ bottom: NIL | horizontal: set(Roof_Ht1,Roof_Ht1*0.5) GableRoof(Index) } }

VaultRoof(n) -->
  case n > 0: roofGable(n*curvedAngleResolution,0,0,false,Index)
              print(n)
              split(y){ (calcSegmentHt(n)): RoofMass(n!=1)
                        comp(f){ bottom: NIL | horizontal: VaultRoof(n-1) } }

DomeRoof(n) -->
  case n > 0: roofHip(n*curvedAngleResolution)
              split(y){ (calcSegmentHt(n)): RoofMass(n!=1)
                        comp(f){ bottom: NIL | horizontal: DomeRoof(n-1) } }
```

Figure 22: Implementation of CGA rules for complex roof types

6.3 Implement user interface for user interaction

Figure 23 represents a GUI implemented to allow users to interactively manipulate 33 parameters related to the 3D building modelling. These parameters encompass various aspects of the 3D modelling process, including visualisation options, building attributes, roof-related attributes, single-dormer attributes, and double-dormer attributes. Table 3 represents all the parameters and their variable names that can be controlled by users within CityEngine GUI.

Table 3: 3D modelling parameters supported by user interface

Parameter category	Parameter name	Remarks
Visualisation options	Representation	Solid colour or realistic representation
	Roof colour	Hexa-decimal colour code
	Wall colour	
	Cleanup	Whether shape errors should be corrected
	Outline status	Add building edges
Building attributes	EvHGT_2	Height of the eave from the ground
	RidgeHeigh	Height of the roof ridge
	AccuRoofFo	Type of the roof
	DrmFrm	Whether a single dormer, double dormer or triple dormer
	DrmDrc	Orientation of the dormer
	DrmRoof	Type of the roof of dormers
	drmRot	Rotate the orientation of the dormer
Roof related attributes	Index	Orientation of the main building roof
	GabHipSid1 / GabHipSid2	The slope of the sides in Gable-hip roofs
	GabHipFrnt	The slope of the front in Gable-hip roofs
	Saltbox_ratio	Ratio of the division in Saltbox roofs
Dormer related attributes	(Sng/Db)DrmLen	Length (Width if the index is 1) of the dormer
	(Sng/Db)DrmWid	Width (Length if the index is 1) of the dormer
	(Sng/Db)DrmHgt	Height of the dormer
	(Sng/Db)DrmbdHt	Dormer body height
	(Sng/Db)DrmDtEd	Distance to the dormer from the roof edge
	(Sng/Db)DrmDtEv	Distance to the dormer from the roof eave
	(Sng/Db)DrmHtEv	Height to the dormer bottom from eave
	(Sng/Db)DrmAngl	Dormer roof slope

Double - Dormer attributes		Single - Dormer attributes	
DblDrmLen	2	SngDrmLen	2
DblDrmWid	2	SngDrmWid	2
DblDrmHgt	2	SngDrmHgt	2
DblDrmBdHt	2	SngDrmBdHt	2
DblDrmDtEd	0 (Object)	SngDrmDtEd	0 (Object)
DblDrmDtEv	0 (Object)	SngDrmDtEv	0 (Object)
DblDrmHtEv	0 (Object)	SngDrmHtEv	0 (Object)
DblDrmAnagl	63.434949	SngDrmAnagl	63.434949
Roof related attributes		Building Attributes	
PrptHgt	0 (Object)	EvHgt_2	3.169876 (Object)
Index	0 (Object)	RidgeHeigh	3.391194 (Object)
GabHipSid1	0 (Object)	AccuRoofFo	GableHip
GabHipSid2	0 (Object)	DrmFrm	TripleDormer
GabHipFrnt	0 (Object)	DrmDrc	0
saltbox_ratio	0.333	BID	166 (Object)
Visualization Options		DrmRoof	Hip
Representation	solid color	drmRot	0 (Object)
RoofColour	#A67B5B		
WallColour	#F5F5DC		
Cleanup	TRUE		
Outlinestatus	FALSE		

Figure 23: GUI parameters for 3D modelling

6.4 Generate LOD2 model

After conducting the previous processing steps inside ArcGIS Pro, the generation of the LOD2 model was conducted in Esri CityEngine. The process is carried out through a series of systematic steps aimed at creating accurate and visually compelling representations of the study area.

Step 1: The process commences with the importation of essential geospatial data, including pre-processed shapefiles delineating building footprints with supplementary information, DEM capturing terrain elevations, and orthophotos providing aerial imagery. This data serves as the foundational framework for the subsequent modelling.

Step 2: The imported shapefiles are aligned to the terrain to ensure spatial accuracy in the generated 3D models. This alignment process facilitates the proper placement of building structures atop the terrain surface, ensuring that the models conform to the underlying topography captured by the DEM.

Step 3: As captured in Figure 15, CGA rule parameters are linked with shapefile attributes. This crucial step enables the automated generation of 3D building models based on predefined rules and attribute values derived from the shapefile data. By establishing this linkage, the generation process becomes highly adaptable and responsive to variations in building attributes. However, if the parameter and attribute name are the same, this step will be applied automatically once the CGA rule file is applied to the shapefile.

Step 4: The generated 3D models undergo refinement using additional parameters mentioned in Table 3 to enhance their realism and accuracy. This refinement stage may involve adjustments to building heights, roof styles, facade textures, and other architectural details such as dormers. By fine-tuning these parameters, the 3D models achieve a higher level of fidelity and coherence, closely resembling real-world structures. Figure 24 illustrates some of the dormers added during the final refinement stage.

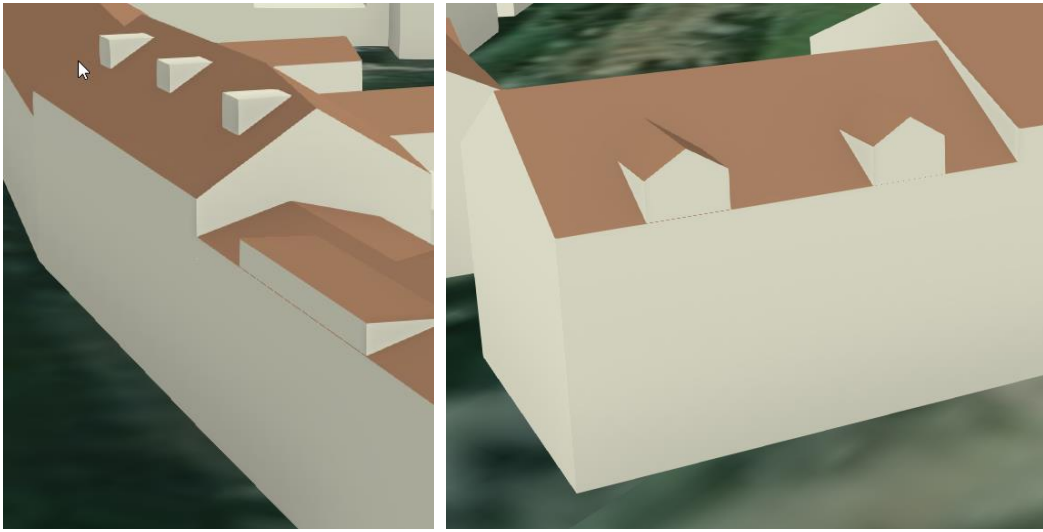


Figure 24: Dormers added during final refinement stage.

7 ACCURACY ASSESSMENT

7.1 Accuracy assessment of ridge height

Ridge height, which is the height of the roof from ground level, is calculated based on a statistical methodology proposed by Hron and Halounová (2019), which involves using the 95th percentile as the top height value within the footprint. However, in addition to the 95th percentile, three more statistical values were considered in this study to evaluate the most accurate metrics.

To validate the accuracy of the proposed methodology, an extensive accuracy assessment is conducted. This assessment involves comparing the ridge height values generated through the statistical methodology against manually digitised values. By juxtaposing these two sets of data, it was evaluated how close each method was to the actual value of the ridge height. Figures 25, 26, and 27 represent the Absolute Error distribution of each study area for each method of consideration. According to the error distribution, it is evident that in all three study areas, there are some building footprints which have extreme RMSEs.

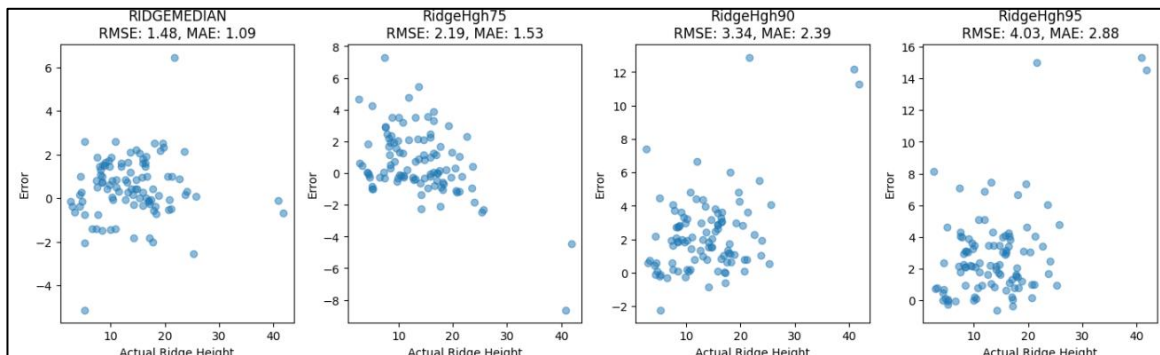


Figure 25: City area ridge height absolute error distribution.

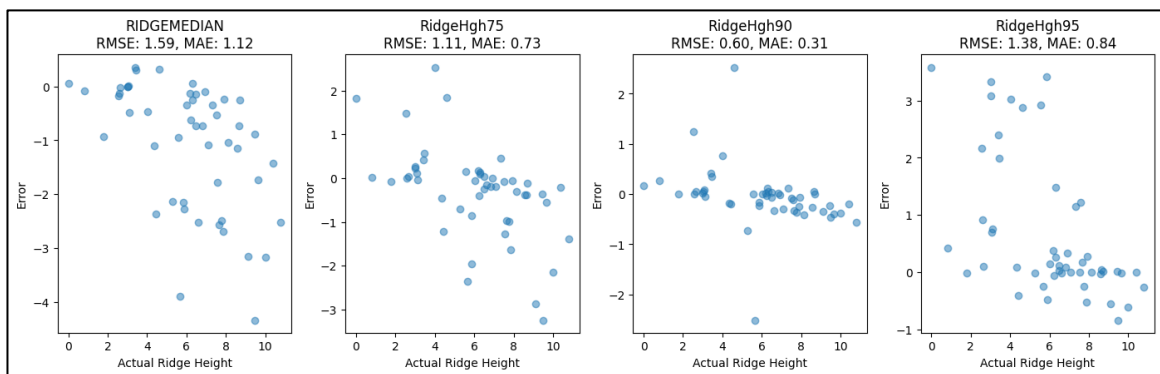


Figure 26: Rural area ridge height absolute error distribution.

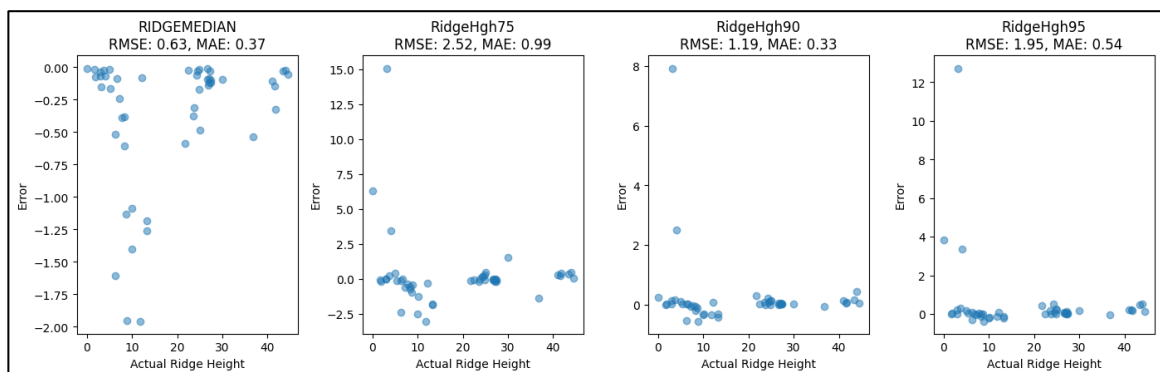


Figure 27: Residential area ridge height absolute error distribution

Figure 28 represents the RMSE of each study area for each method of ridge height calculation. Overall, ridge height calculation by median gives the least error for residential and city centres. However, in rural areas, calculating ridge height by the 90th percentile gives a lower RMSE, around 1m less than the median method.

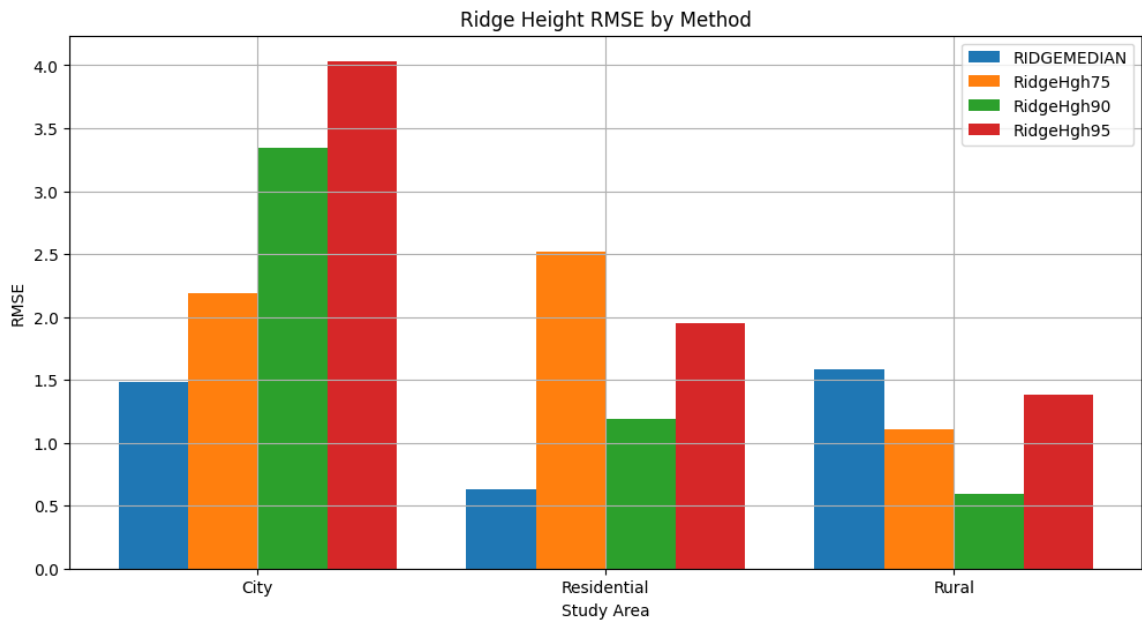


Figure 28: RMSE before removing outliers

After using the 95th percentile to identify and eliminate outliers, a notable improvement was observed in the RMSE values (Figure 29). Across all study areas, the removal of outliers led to a substantial reduction in RMSE, bringing it closer to 1 meter for rural and urban locales while achieving less than 0.5 meters for residential regions. Interestingly, upon outlier removal, the method based on the 90th percentile for ridge height estimation exhibited the lowest RMSE for rural and residential areas, averaging around 0.25 meters. However, for urban areas, the RMSE remained relatively high, approximately 2.5 meters.

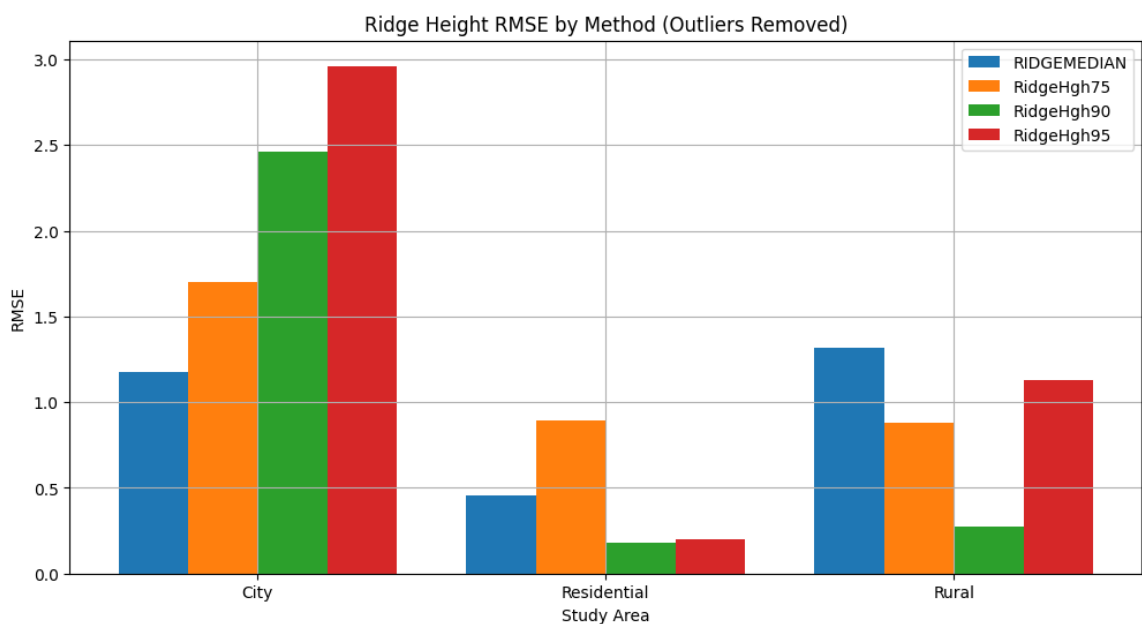


Figure 29: RMSE after removing outliers

The median method was selected for calculating ridge height due to its inherent stability and consistently low RMSE values, both before and after the removal of outliers. Even though outlier removal resulted in lower RMSE values for ridge height estimation based on the 90th percentile, the median method maintained its appeal due to its reliability and relatively stable performance across all scenarios.

7.2 Accuracy assessment of eave height

Eave height, which is the height of the roof bottom from ground level, is calculated using a statistical methodology proposed by Hron and Halounová (2019). However, in addition to the 75th percentile, three more statistical values were considered in this study to evaluate the most accurate metrics for eave height calculation.

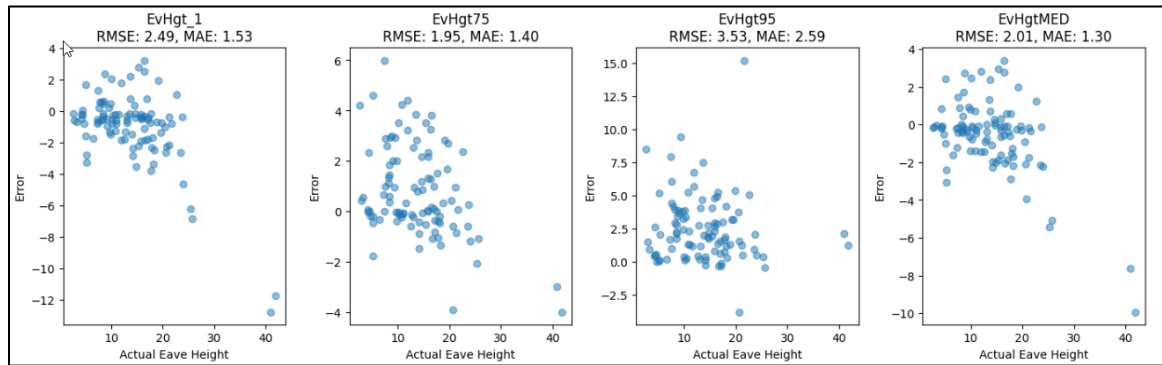


Figure 30: City area eave height absolute error distribution

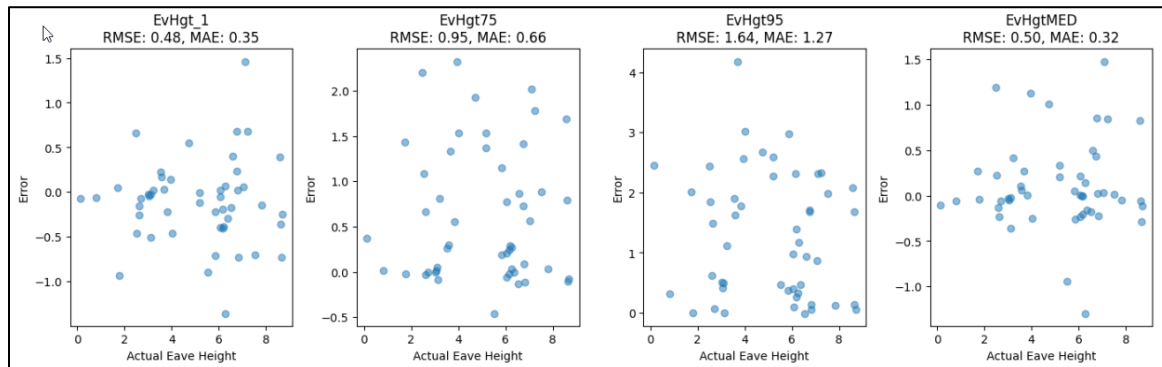


Figure 31: Rural area eave height absolute error distribution

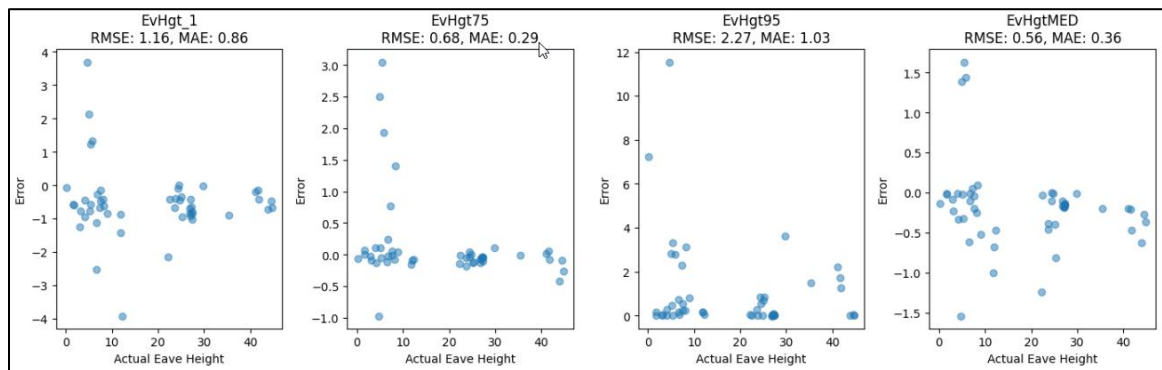


Figure 32: Residential area eave height absolute error distribution

Based on the observations from Figures 30, 31, and 32, it becomes apparent that outliers are present across all scenarios when calculating eave height using each statistical method, as outlined in the methodology section. These outliers, which deviate significantly from most data points, can potentially skew the estimation process and lead to inaccuracies in the results. This highlights the importance of identifying and addressing outliers to ensure the robustness and reliability of the eave height calculation methodology.

Figures 33 and 34 represent a comparison of different eave height calculation methods before and after removing outliers. Accordingly, it is evident that in all cases, the city centre study area accounted for the highest RMSE. Apart from that, it is also important to point out that in almost all cases, using the median to calculate eave height is more consistent and accurate, except for the city centre, where the third percentile's RMSE is slightly lower than using the Median. According to Figure 34, a substantial reduction in RMSE is evident across all study areas. Post-outlier removal, RMSE values for the Median method outperform the 75th percentile, except for the residential region.

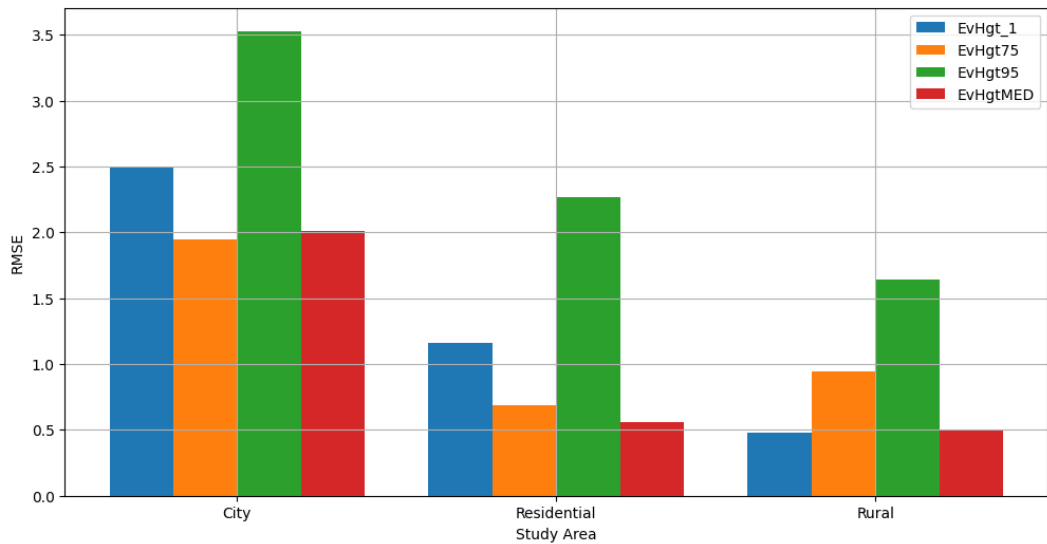


Figure 33: Eave height RMSE before removing outliers

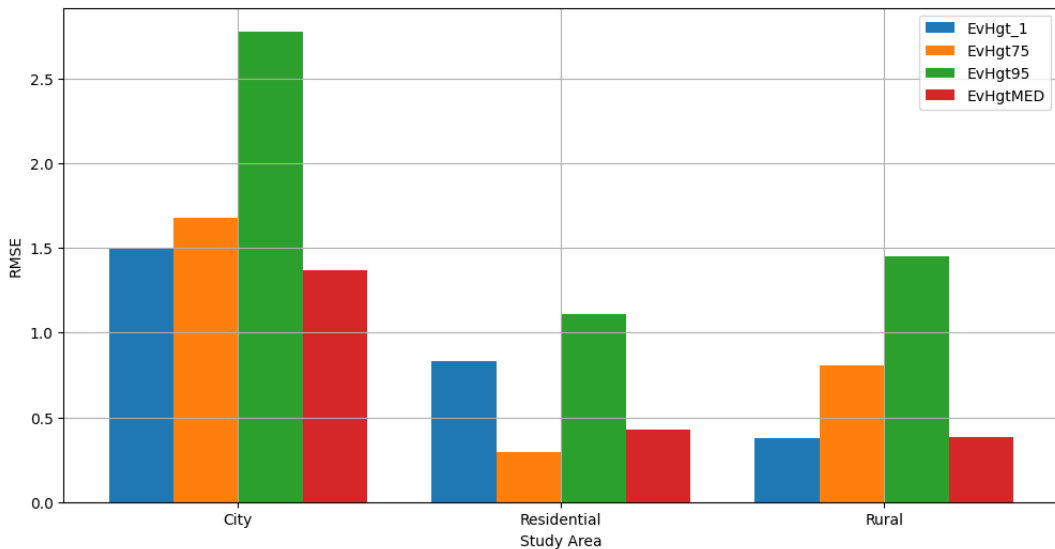


Figure 34: Eave height RMSE after removing outliers

As a result, using the median approach produces the best results for ridge height and eave height calculations. This assumption is substantiated by the significant drop in RMSE found across several study areas prior to and following outlier elimination. The Median method typically outperforms other statistical approaches, including the 75th percentile, across areas. Although the 75th percentile outperforms marginally in residential areas, in other areas, the median technique outperforms it significantly. As a result, in this study, the median will be utilised as the preferred option for estimating ridge and eave heights in the context of 3D building modelling.

7.3 Accuracy assessment of roof type classification

In this section, a thorough evaluation is conducted for each roof type across different study areas. By analysing these metrics, it is possible to gain insights into the model's effectiveness in correctly identifying various roof types and assess any potential biases or challenges encountered during the classification process. Figure 35 represents confusion matrices calculated for each study area.

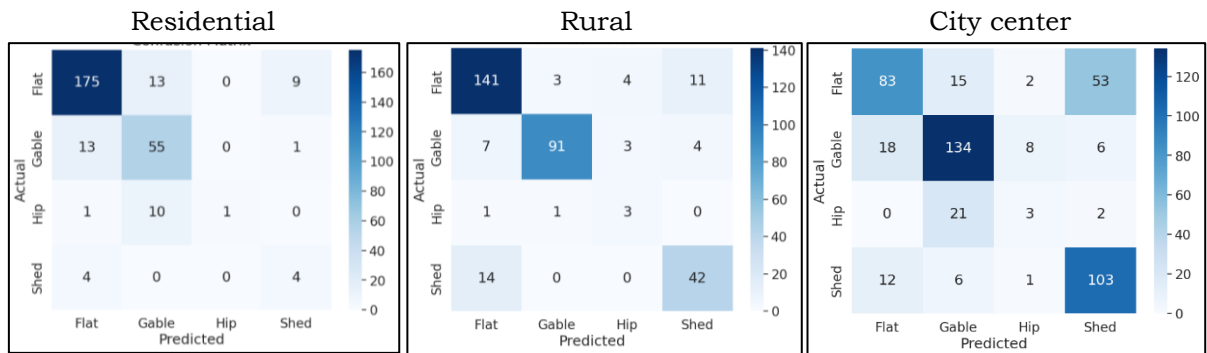


Figure 35: Confusion matrix of each region

7.3.1 Residential area

In the Residential region, the classification results exhibit varying levels of accuracy across different roof types. Most roofs in this area are categorised as flat, which demonstrates a high producer's accuracy (PA) of approximately 0.89, indicating that the classification model effectively identifies Flat roofs when they are present. However, it's important to note that the user's accuracy (UA) for Flat roofs is slightly lower at around 0.91, suggesting that there may be some misclassification of other roof types as Flat. For Gable roofs, while the PA is reasonable at 0.80, the UA is notably lower at approximately 0.71. This indicates that while the model correctly identifies many Gable roofs, there is a higher likelihood of misclassifying other roof types as Gable. The classification of Hip roofs shows a particularly low PA of around 0.08, suggesting that the model struggles to accurately identify Hip roofs when they are present. However, the UA for Hip roofs is perfect (1.0), indicating that when the model predicts a Hip roof, it is almost always correct. Regarding Shed roofs, the PA is moderate at 0.50, indicating that the model correctly identifies approximately half of the Shed roofs present. However, the UA is lower at approximately 0.29, suggesting that there is a higher rate of misclassification of other roof types as Shed.

7.3.2 Rural area

In the Rural region, the classification results display varying accuracies across different roof types. The abundance of Flat roofs is accurately captured by the model,

with a high PA of approximately 0.89 and a respectable UA of around 0.87. This indicates that the model effectively identifies Flat roofs when they are present and maintains a high level of accuracy in its predictions. Similarly, for Gable roofs, the model demonstrates a high PA of around 0.87 and a strong UA of approximately 0.96. This suggests that the classification model effectively identifies Gable roofs and maintains a high level of accuracy in its predictions for this roof type. Hip roofs exhibit lower accuracies compared to Flat and Gable roofs, with a PA of 0.60 and a UA of 0.30. This indicates that while the model identifies some Hip roofs correctly, there is room for improvement in accurately classifying this roof type. Shed roofs also show reasonably good accuracy metrics, with a PA of 0.75 and a UA of approximately 0.74. This suggests that the model is relatively successful in identifying Shed roofs, although there is still room for improvement.

7.3.3 City Centre area

In the City Centre, the classification accuracies vary across different roof types, with noticeable differences compared to the Residential and Rural regions. The model's performance in identifying Flat roofs is relatively weak, with a PA of approximately 0.54 and a UA of around 0.73. This suggests that there is a higher rate of misclassification of other roof types as Flat in this area. For Gable roofs, the model demonstrates a high PA of around 0.81, indicating that it effectively identifies Gable roofs when they are present. However, the UA is slightly lower at approximately 0.76, suggesting some misclassification of other roof types, such as Gable. Hip roofs exhibit the lowest accuracy metrics in this region, with a PA of 0.12 and a UA of 0.21. This indicates that the model struggles to accurately identify Hip roofs when they are present, leading to a higher rate of misclassification. Shed roofs, on the other hand, show relatively good accuracy metrics, with a PA of approximately 0.84 and a UA of around 0.63. This suggests that the model is relatively successful in identifying Shed roofs, although there is still room for improvement.

In summary, the classification performance varies across different roof types and regions. While the model demonstrates high accuracy in identifying certain roof types such as Flat and Gable in the Residential and Rural regions, it struggles with accurate classification of Hip roofs, particularly in the City Centre. Shed roofs generally exhibit moderate accuracy across all regions, indicating room for improvement in the model's ability to classify this roof type accurately.

8 IMPLEMENTATION OF THE WORKFLOW

One of the primary goals of this study is to provide a systematic workflow that will allow users to easily traverse through the procedures needed in designing complicated roof kinds utilising CGA rules. While the intricacy of the models remains inherent, the goal is to shield users from those models, allowing them to easily comprehend the process and execute it.

To achieve this, Esri tasks were used, a recently added feature in ArcGIS Pro. By incorporating Esri tasks into the workflow, users have access to optimised procedures and intuitive interfaces that enable the execution of complicated models and Python scripts without revealing their complexity. This method ensures that users can easily traverse the implementation process step by step. Figure 36 demonstrates the implemented workflow, which has five main stages. Each of these stages is built with sub-tasks and provides information and instructions for the users.

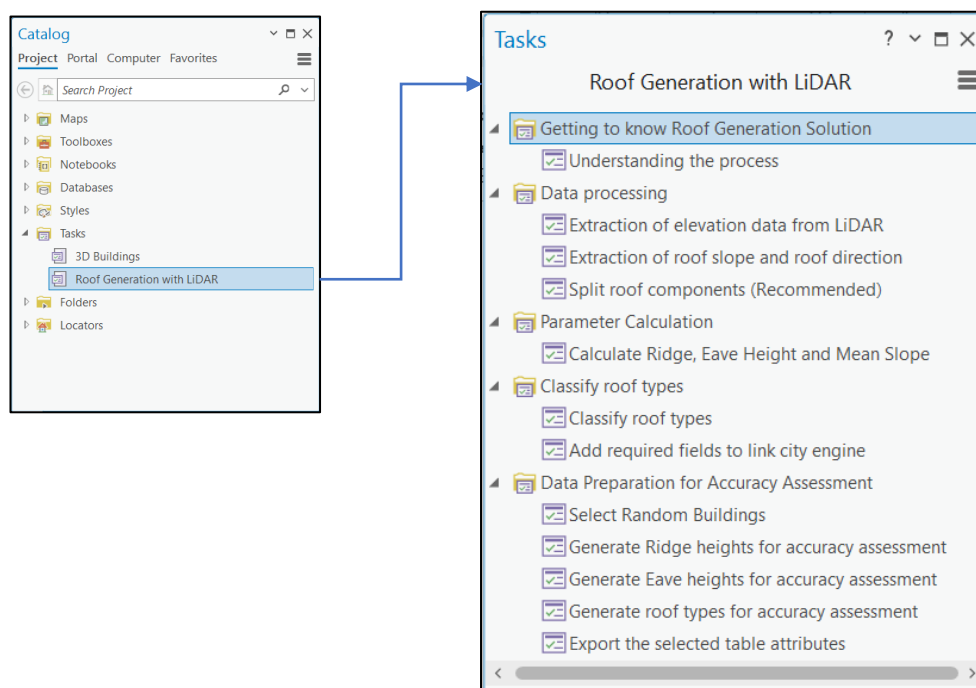


Figure 36: Implemented pipeline to streamline the workflow

9 RESULTS

9.1 Results of roof parameters calculation

This thesis details a comprehensive workflow aimed at automating the generation and classification of complex roof types through the integration of geospatial data processing techniques and CGA principles. The parameter calculation stage, outlined in section 4, plays a fundamental role in preparing the geospatial data for subsequent analysis. In this stage, NDSM is extracted from LiDAR data and generates the flow direction and slope of the area. In section 4.2, the analysis experiment uses multiple methods for calculating slope, ridge height, and eave height. Tables 4 and 5 demonstrate a summarised RMSE and MAE of different methods used to calculate ridge height and eave height.

Table 4: Ridge height calculation results

Ridge Height	RMSE		City	Residential	Rural
		Median	1.484	0.634	1.586
		75th Percentile	2.186	2.518	1.107
		90th percentile	3.340	1.192	0.596
		95th percentile	4.034	1.949	1.380
	MAE	Median	1.093	0.371	1.120
		75th Percentile	1.531	0.991	0.725
		90th percentile	2.394	0.332	0.311
		95th percentile	2.877	0.537	0.837

Table 5: Eave height calculation results

Eave Height	RMSE		City	Residential	Rural	
		Method 1 (Median)		2.494	1.164	0.482
		Method 2	Median	2.013	0.560	0.496
			75th percentile	1.949	0.684	0.947
			95th percentile	3.528	2.266	1.639
	MAE	Method 1 (Median)		1.532	0.855	0.346
		Method 2	Median	1.296	0.365	0.320
			75th percentile	1.403	0.289	0.658
			95th percentile	2.589	1.028	1.275

Choosing the most effective slope indicator is also an important part of the procedure. Four statistical approaches were tested to establish the most efficient slope indicator, and accuracy scores were compared. By comparing f-scores at different thresholds, Mean and Median indicators were shown to be the most dependable, with Median marginally surpassing Mean in all research areas. Figure 18 and Table 2 show the accuracy values obtained for each method.

9.2 Results of the LOD2 model

In this section, the primary outputs of our research are presented: LOD2 models of three distinct study areas – the City Centre, Rural, and Residential regions. These models could be considered as the final output of the implemented workflow, showing a comprehensive representation of urban landscapes.

Figure 37 depicts six photos of LOD2 models chosen to demonstrate each research location's various architectural typologies and contextual details. Each study region is represented by two photos that provide different viewpoints of building representations using solid textures and realistic textures. The lifelike textures are not a true depiction of reality. However, it is merely to emphasise the built model's capacity to include genuine textures acquired as photographs of real-life facades and roofs. The photos with solid textures provide a simple but useful representation of the built environment, emphasising the spatial distribution and structure of buildings in the study region. In contrast, pictures with realistic textures create a vivid and immersive depiction of the study regions, resulting in a more lifelike visualisation.

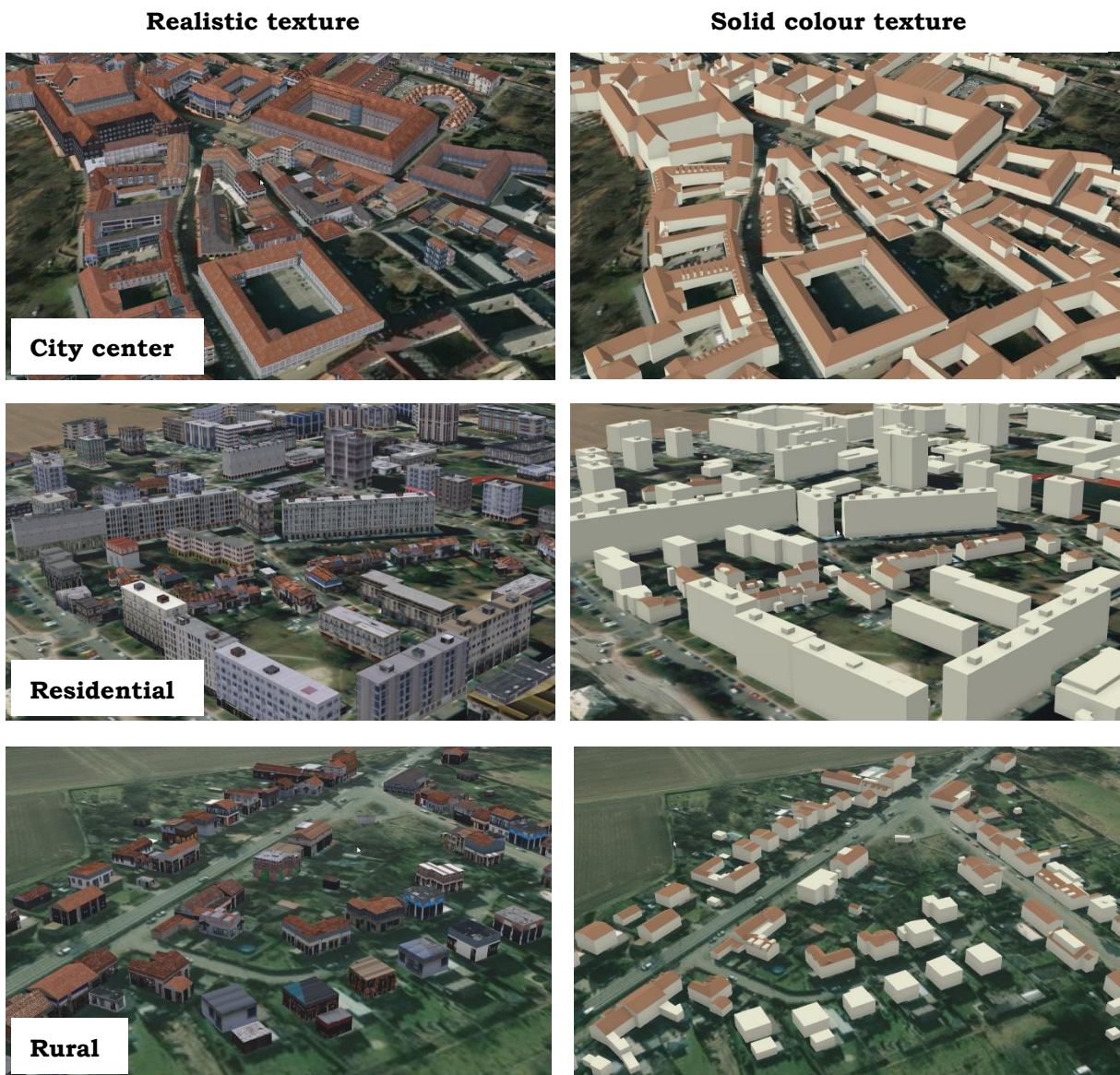


Figure 37: Sample buildings generated from the pipeline.

10 DISCUSSION

The methodology adopted for the calculation of ridge height occasionally yields unusually high outliers, which can be attributed to several factors. One prominent reason is the presence of natural and man-made features within the building footprint, such as towers, trees, and other components. These features can significantly affect the calculation of ridge height, particularly when they extend above the roofline of the building. As a result, the algorithm may erroneously attribute the height of these features to the ridge height, leading to inflated measurements. However, as shown in the accuracy assessment, by taking the Median values as a statistical measure, most of these outliers can be reduced. Furthermore, inaccuracies stemming from blunders during the digitisation of building footprints contribute to the occurrence of outliers in ridge height calculations. In some cases, the actual footprint area of the building may be smaller than the digitised area due to errors in delineating the boundaries of the building (Figure 38). Consequently, the methodology may inaccurately estimate the ridge height based on the larger digitised footprint area, resulting in exaggerated measurements.

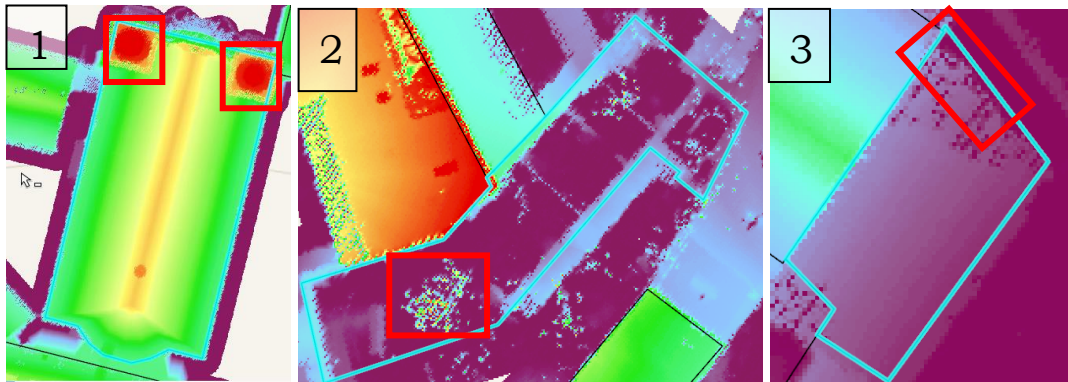


Figure 38: Building footprints with extreme RMSEs for ridge height.

In the work of Hron and Halounová (2019), they suggested and used the 95th percentile for ridge height calculation; however, in this study, the same parameter gave the highest RMSE for city centre ridge height calculation. In the case of rural and residential regions, it did not perform considerably as well. Since the median performed well in terms of RMSE, it is recommended to use it for calculating ridge height across three different study areas. When calculating the eaves height, they recommended using a buffer on both sides of the building footprint with the third percentile. The accuracy assessment showed that constructing a buffer on both sides of the footprint generates a much higher RMSE than creating a buffer solely inside the footprint boundary when the results were compared with the buffer built exclusively inside.

In the process of modelling complex buildings, it is often necessary to incorporate additional components within the building footprint, such as dormers and roof drains. These architectural features play crucial roles in the functionality and aesthetic of the building but are not always adequately represented in the initial building footprint data. As a result, the omission of dormers, roof drains, and similar elements can lead to inaccuracies in the building model. To address these challenges, it becomes necessary to manually add these additional components within the building footprint during the modelling process. Figure 39 demonstrates a comparison of the original building footprint (green colour) and the updated footprint (red colour) to address these complexities. As a result of splitting the roof into distinct components, this segmentation often results in variations in both eave height and ridge height across these components. Consequently,

it becomes necessary to adjust these heights to ensure uniformity and coherence among the different parts of the same roof within the City Engine.

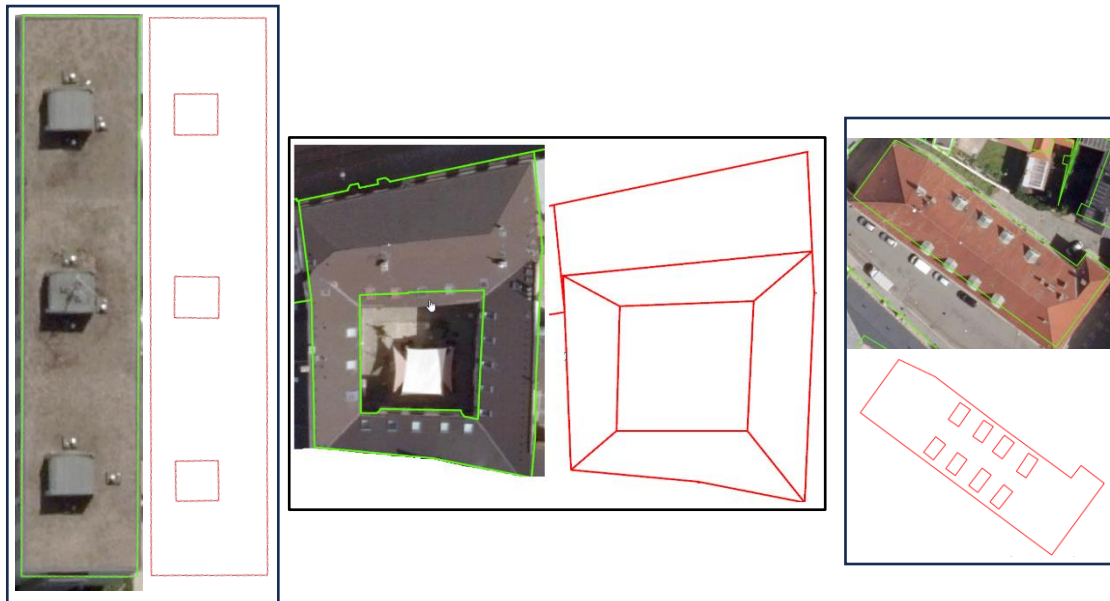


Figure 39: Comparison of before and after building footprint update.

The current method employed for roof classification falls short of achieving acceptable accuracy levels, particularly in accurately classifying pitched roof types. To address this limitation, it is imperative to explore alternative approaches that are combined with the current approach and other advanced technologies. One promising avenue for improvement is the adoption of a deep-learning image recognition approach. By training the deep learning model on a diverse dataset containing labelled examples of various roof types, it can learn to recognise key characteristics indicative of pitched roofs with high accuracy. Furthermore, the deep learning approach has the potential to continuously improve over time as it encounters new data.

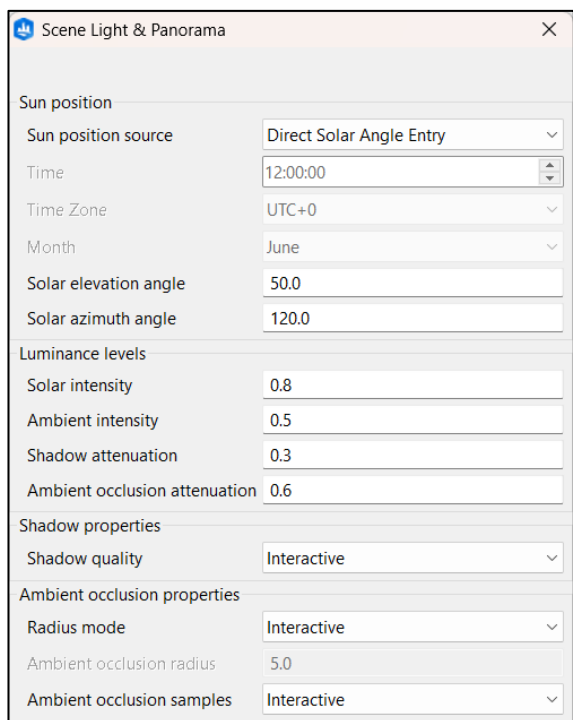


Figure 40: A Building located in high slope area (Laharchitect, 2020)

In certain extreme scenarios, buildings are situated across sloped regions, leading to inconsistencies in eave height despite the eaves being at the same level. As depicted in Figure 40, such situations pose challenges for the created script, particularly in

accommodating varying eave heights within the same building structure. To mitigate this issue, it is advisable to implement a strategy of splitting buildings into distinct sections and applying CGA rules separately to each section. By treating each section independently, we can ensure that eave heights are accurately represented in accordance with the surrounding terrain.

Since its launch in 2004, the Copernicus Atmosphere Monitoring Service (CAMS) has been a vital source of information on solar radiation levels in both cloud-free and actual weather circumstances. To assess the overall solar energy potential of any building, users



may easily merge CAMS solar radiation data with 3D building models created with the provided pipeline. Since solar radiation levels per square meter are provided by CAMS data, an accurate evaluation of each building's ability to generate solar energy may be obtained by multiplying this number by the size of its roof. By enabling stakeholders to recognise and rank buildings with the greatest potential for solar energy generation, this capability maximises the use of solar energy systems. Additionally, as seen in Figure 41, users may dynamically alter the sun's azimuth and angle within the city engine. Using this interactive tool, stakeholders may determine the best places to put solar panels to maximise energy generation efficiency and overall system performance while minimising building shadows.

Figure 41: Sun azimuth and angle

Stakeholders may promote sustainable development practices and stimulate innovation in the energy industry by fusing 3D models with Copernicus solar data. This integration leads to a more effective use of renewable energy resources by improving the accuracy of solar energy evaluations and facilitating informed decision-making processes. In the end, stakeholder cooperation, a 3D model creation pipeline, and CAMS data synergy open the door to a more robust and sustainable energy future.

It is important to draw attention to certain constraints of the methodology. Although the created technique accommodates the majority of the roofs (15 types), there could be situations that limit its application to regions with a wider variety of architectural styles. Furthermore, even with a single footprint, certain structures may have varying altitudes or several types of roofs, which makes manual separation necessary for precise modelling. The current pipeline is designed to automatically identify flat, shed and gable with acceptable accuracy levels. However, the CGA script support modelling 15 different roof types. Therefore, during the building footprint database generation stage end user should manually identify and fill the additional roof types. It can be labour-and time-intensive to manually add many dormers to the building footprint when there are multiple dormers on the roof. It would be ideal to use extra 3D modelling tools, like Sketchup, to model unique, unusual buildings like cathedrals.

The elevation data used to generate 3D models was obtained by analysing a high-density LiDAR point cloud. These models were then translated to coincide with LiDAR-

derived digital elevation models (DEMs). However, when these models were visualised as a scene on the ArcGIS Online platform, there was a clear gap between the ground and the structures. This mismatch is due to the intrinsic accuracy variations between ArcGIS Online terrain and LiDAR-derived terrain. LiDAR technology provides incredibly precise elevation data, but the landscape depiction in ArcGIS Online may lack the same degree of precision and resolution. As a result, disparities between the two datasets might occur, causing visual inconsistencies such as the visible gap between the ground and the structures.

There are several future directions that might be taken to improve the approach and address its drawbacks. First off, adding support for other roof kinds would make the automated building production process more flexible and applicable. This can entail carrying out an in-depth study to find new roof typologies that are frequently observed in urban settings and incorporating them into the current framework. The existing approach to identifying roof types needs to be more accurate. Investigating novel methods with deep learning to automatically detect different types of roofs from aerial photography or LiDAR data is one strategy that may be used. It could be able to create more reliable and accurate categorisation models by utilising machine learning algorithms, which would lessen the need for manual intervention.

11 CONCLUSION

The major goal of this project was to provide a systematic process for automatically generating LOD2 buildings in the city of Olomouc. Specific goals were established, such as determining building roof types, roof components, and building height, as well as creating CGI scripts in Esri CityEngine for building generation automation, assessing the accuracy of the generated 3D roof models, and using the developed model to estimate solar energy potential.

To fulfil these goals, ArcGIS Pro and Esri CityEngine were used, which enabled the building of a reusable CGA script. This script assisted in the automatic production of structures by identifying roof kinds, components, and building height.

The study findings provide substantial contributions to the disciplines of Geographic Information Systems (GIS) and 3D building modelling in urban environments. The developed procedure allows for the creation of LOD2 building models, which may be used for a variety of applications, including 3D geovisualization, solar energy cadastre preparation, noise propagation study, and other research critical for urban decision-making. The outputs will be immediately used for a scientific project of the Czech Ministry of Culture, "Olomouc in 3D - A New Dimension of the City's Cultural Heritage: Past, Present, Future".

This work established the feasibility and efficacy of the approach for autonomously producing LOD2 buildings in Olomouc. The objectives were met by devising a methodical strategy, writing reusable CGI scripts, and evaluating the correctness of created 3D roof models. Furthermore, the research opens the door to a wide range of applications, ultimately leading to better urban planning and decision-making processes.

To sum up, this research marks a significant milestone in the field of urban modelling and analysis, providing a robust and adaptable methodology for generating LOD2 buildings in Olomouc and beyond. By leveraging advanced GIS technologies and computational tools, this study has not only addressed current challenges in building generation but has also paved the way for future advancements in the field.

REFERENCES AND INFORMATION SOURCES

- Ahmed, S.F. *et al.* (2023) 'Deep learning modelling techniques: current progress, applications, advantages, and challenges', *Artificial Intelligence Review*, 56(11), pp. 13521–13617. Available at: <https://doi.org/10.1007/s10462-023-10466-8>.
- Alam, W. (2011) 'GIS based Assessment of Noise Pollution in Guwahati City of Assam, India', *International Journal on Environmental Sciences* [Preprint]. Available at: <https://www.semanticscholar.org/paper/GIS-based-Assessment-of-Noise-Pollution-in-Guwahati-Alam/aac0ae6a81ba003f9750ff7a407c5064288e0bce> (Accessed: 6 November 2023).
- Al-Bilbisi, H. (2019) 'Spatial Monitoring of Urban Expansion Using Satellite Remote Sensing Images: A Case Study of Amman City, Jordan', *Sustainability*, 11(8), p. 2260. Available at: <https://doi.org/10.3390/su11082260>.
- Alizadehashrafi, B. (2015) 'Using parameters of dynamic pulse function for 3d modeling in lod3 based on random textures', *The International Archives of the Photogrammetry, Remote Sensing and Spatial Information Sciences*, XL-1-W5, pp. 51–55. Available at: <https://doi.org/10.5194/isprsarchives-XL-1-W5-51-2015>.
- Allen, J.B. and Berkley, D.A. (1979) 'Image method for efficiently simulating small-room acoustics', *The Journal of the Acoustical Society of America*, 65(4), pp. 943–950. Available at: <https://doi.org/10.1121/1.382599>.
- American Legal Publishing (n.d.) *6.100 HEIGHT.*, *American Legal Publishing*. Available at: https://codelibrary.amlegal.com/codes/ftworth/latest/ftworth_tx/0-0-0-38192 (Accessed: 4 January 2024).
- Badwi, I.M., Ellaithy, H.M. and Youssef, H.E. (2022) '3D-GIS Parametric Modelling for Virtual Urban Simulation Using CityEngine', *Annals of GIS*, 28(3), pp. 325–341. Available at: <https://doi.org/10.1080/19475683.2022.2037019>.
- Bagheri, H., Schmitt, M. and Zhu, X. (2019) 'Fusion of Multi-Sensor-Derived Heights and OSM-Derived Building Footprints for Urban 3D Reconstruction', *ISPRS International Journal of Geo-Information*, 8(4), p. 193. Available at: <https://doi.org/10.3390/ijgi8040193>.
- Bassier, M., Vergauwen, M. and Van Genechten, B. (2017) 'Automated classification of heritage buildings for as-built bim using machine learning techniques', *ISPRS Annals of the Photogrammetry, Remote Sensing and Spatial Information Sciences*, IV-2-W2, pp. 25–30. Available at: <https://doi.org/10.5194/isprs-annals-IV-2-W2-25-2017>.
- Bernard, J. *et al.* (2022) 'Estimation of missing building height in OpenStreetMap data: a French case study using GeoClimate 0.0.1', *Geoscientific Model Development*, 15(19), pp. 7505–7532. Available at: <https://doi.org/10.5194/gmd-15-7505-2022>.
- Biljecki, F. *et al.* (2021) 'Open government geospatial data on buildings for planning sustainable and resilient cities'. arXiv. Available at: <https://doi.org/10.48550/arXiv.2107.04023>.
- Blaschke, T. (2010) 'Object based image analysis for remote sensing', *ISPRS Journal of Photogrammetry and Remote Sensing*, 65(1), pp. 2–16. Available at: <https://doi.org/10.1016/j.isprsjprs.2009.06.004>.
- Borkowski, A. and Jóźków, G. (2012) 'Accuracy assessment of building models created from laser scanning data', *The International Archives of the Photogrammetry, Remote Sensing and Spatial Information Sciences*, XXXIX-B3, pp. 253–258. Available at: <https://doi.org/10.5194/isprsarchives-XXXIX-B3-253-2012>.

- Cai, B. *et al.* (2023) ‘Deep learning-based building height mapping using Sentinel-1 and Sentinel-2 data’, *International Journal of Applied Earth Observation and Geoinformation*, 122, p. 103399. Available at: <https://doi.org/10.1016/j.jag.2023.103399>.
- Cai, M., Yao, Y. and Wang, H. (2018) ‘Urban Traffic Noise Maps under 3D Complex Building Environments on a Supercomputer’, *Journal of Advanced Transportation*, 2018, p. e7031418. Available at: <https://doi.org/10.1155/2018/7031418>.
- Canaz Sevgen, S. and Karsli, F. (2020) ‘An improved RANSAC algorithm for extracting roof planes from airborne lidar data’, *The Photogrammetric Record*, 35(169), pp. 40–57. Available at: <https://doi.org/10.1111/phor.12296>.
- Cao, Y. and Huang, X. (2021) ‘A deep learning method for building height estimation using high-resolution multi-view imagery over urban areas: A case study of 42 Chinese cities’, *Remote Sensing of Environment*, 264, p. 112590. Available at: <https://doi.org/10.1016/j.rse.2021.112590>.
- Chafiq, T. *et al.* (2021) ‘U-Net: Deep Learning for Extracting Building Boundary Collected by Drone of Agadir’s Harbor’, in S. Motahhir and B. Bossoufi (eds) *Digital Technologies and Applications*. Cham: Springer International Publishing (Lecture Notes in Networks and Systems), pp. 111–121. Available at: https://doi.org/10.1007/978-3-030-73882-2_11.
- Chen, H. *et al.* (2021) ‘Plane segmentation for a building roof combining deep learning and the RANSAC method from a 3D point cloud’, *Journal of Electronic Imaging*, 30(5), p. 053022. Available at: <https://doi.org/10.1117/1.JEI.30.5.053022>.
- Cheng, X. *et al.* (2023) ‘Application of Deep Learning in Multitemporal Remote Sensing Image Classification’, *Remote Sensing*, 15(15), p. 3859. Available at: <https://doi.org/10.3390/rs15153859>.
- Cheuk, M.L. and Yuan, M. (2009) ‘Assessing Spatial Uncertainty of Lidar-derived Building Model’, *Photogrammetric Engineering & Remote Sensing*, 75(3), pp. 257–269. Available at: <https://doi.org/10.14358/PERS.75.3.257>.
- Chi, M. *et al.* (2016) ‘Big Data for Remote Sensing: Challenges and Opportunities’, *Proceedings of the IEEE*, 104(11), pp. 2207–2219. Available at: <https://doi.org/10.1109/JPROC.2016.2598228>.
- Chiabrandò, F. *et al.* (2017) ‘3D roof model generation and analysis supporting solar system positioning’, *GEOMATICA*, 71(3), pp. 137–153. Available at: <https://doi.org/10.5623/cig2017-301>.
- Cui, S., Yan, Q. and Reinartz, P. (2012) ‘Complex building description and extraction based on Hough transformation and cycle detection’, *Remote Sensing Letters*, 3(2), pp. 151–159. Available at: <https://doi.org/10.1080/01431161.2010.548410>.
- ČÚZK (2023) *ČÚZK - Open data - basic information*. Available at: <https://www.cuzk.cz/Uvod/Produkty-a-sluzby/Otevrena-data/Otevrena-data-zakladni-informace.aspx> (Accessed: 3 January 2024).
- Danilina, N., Slepnev, M. and Chebotarev, S. (2018) ‘Smart city: automatic reconstruction of 3D building models to support urban development and planning’, *MATEC Web of Conferences*, 251, p. 03047. Available at: <https://doi.org/10.1051/mateconf/201825103047>.
- Deng, Y., Cheng, J.C.P. and Anumba, C. (2016) ‘A framework for 3D traffic noise mapping using data from BIM and GIS integration’, *Structure and Infrastructure Engineering*, 12(10), pp. 1267–1280. Available at: <https://doi.org/10.1080/15732479.2015.1110603>.

DigitalGlobe (2017) *Technical Specification Ecopia Building Footprints Powered by DigitalGlobe*. Digital Globe, p. 14. Available at: https://dg-cms-uploads-production.s3.amazonaws.com/uploads/legal_document/file/109/DigitalGlobe_Ecopia_Building_Footprints_Technical_Specification.pdf.

Donges, N. (2022) *What Is Transfer Learning? A Guide for Deep Learning | Built In, What Is Transfer Learning? Exploring the Popular Deep Learning Approach*. Available at: <https://builtin.com/data-science/transfer-learning> (Accessed: 2 January 2024).

ECC (n.d) 'Building footprint', *Building footprint*. Available at: <https://constructioncosts.eu/glossary/building-footprint/> (Accessed: 4 January 2024).

Edvardsson, K.N. (2013) *3D GIS modelling using ESRI's CityEngine: a case study from the University Jaume I in Castellon de la Plana Spain*. masterThesis. Available at: <https://run.unl.pt/handle/10362/9198> (Accessed: 5 January 2024).

Erener, A., Sarp, G. and Karaca, M.I. (2020) 'An approach to urban building height and floor estimation by using LiDAR data', *Arabian Journal of Geosciences*, 13(19), p. 1005. Available at: <https://doi.org/10.1007/s12517-020-06006-1>.

Eschenbach, W.J. von (2021) 'Transparency and the Black Box Problem: Why We Do Not Trust Ai', *Philosophy and Technology*, 34(4), pp. 1607–1622. Available at: <https://doi.org/10.1007/s13347-021-00477-0>.

Esri (2015) *Geodesign Toolkit: CityEngine-GIS Integration Tools*, *Esri Community*. Available at: <https://community.esri.com/t5/arcgis-cityengine-documents/geodesign-toolkit-cityengine-gis-integration-tools/ta-p/916972> (Accessed: 5 January 2024).

Esri (2023) *Introduction to 3D Buildings—ArcGIS Solutions | Documentation*. Available at: <https://doc.arcgis.com/en/arcgis-solutions/latest/reference/introduction-to-3d-buildings.htm> (Accessed: 5 January 2024).

Esri (n.d.a) *How Flow Direction works—ArcGIS Pro | Documentation*. Available at: https://pro.arcgis.com/en/pro-app/latest/tool-reference/spatial-analyst/how-flow-direction-works.htm#ESRI_SECTION1_2A42BFCB9D6440D2970535F396CED22B (Accessed: 4 January 2024).

Esri (n.d.b) *Introduction to ArcGIS Pro—ArcGIS Pro | Documentation*. Available at: <https://pro.arcgis.com/en/pro-app/latest/get-started/get-started.htm> (Accessed: 5 January 2024).

Esri (n.d.c) *What is a task?—ArcGIS Pro | Documentation*. Available at: <https://pro.arcgis.com/en/pro-app/3.0/help/tasks/whatistask.htm> (Accessed: 30 March 2024).

Esri R&D Center Zurich (2010) *CityEngine_cga/Building_From_Footprint.cga at master · jbdong/CityEngine_cga, GitHub*. Available at: https://github.com/jbdong/CityEngine_cga/blob/master/Building_From_Footprint.cga (Accessed: 13 May 2024).

Fischler, M.A. and Bolles, R.C. (1981) 'Random sample consensus: a paradigm for model fitting with applications to image analysis and automated cartography', *Communications of the ACM*, 24(6), pp. 381–395. Available at: <https://doi.org/10.1145/358669.358692>.

Franz, M., Scholz, M. and Hinz, O. (2015) *2D versus 3D Visualizations in Decision Support - The Impact of Decision Makers' Perceptions*.

- Gabara, G. and Sawicki, P. (2021) 'Quality evaluation of 3d building models based on low-altitude imagery and airborne laser scanning point clouds', *The International Archives of the Photogrammetry, Remote Sensing and Spatial Information Sciences*, XLIII-B2-2021, pp. 345–352. Available at: <https://doi.org/10.5194/isprs-archives-XLIII-B2-2021-345-2021>.
- Gergelova, M.B. *et al.* (2020) 'Identification of Roof Surfaces from LiDAR Cloud Points by GIS Tools: A Case Study of Lučenec, Slovakia', *Sustainability*, 12(17), p. 6847. Available at: <https://doi.org/10.3390/su12176847>.
- Girindran, R. *et al.* (2020) 'On the Reliable Generation of 3D City Models from Open Data', *Urban Science*, 4(4), p. 47. Available at: <https://doi.org/10.3390/urbansci4040047>.
- Gönültaş, F., Atik, M.E. and Duran, Z. (2020) 'Extraction of Roof Planes from Different Point Clouds Using RANSAC Algorithm', *International Journal of Environment and Geoinformatics*, 7(2), pp. 165–171. Available at: <https://doi.org/10.30897/ijgeo.715510>.
- Haklay, M. (2010) 'How Good is Volunteered Geographical Information? A Comparative Study of OpenStreetMap and Ordnance Survey Datasets', *Environment and Planning B: Planning and Design*, 37(4), pp. 682–703. Available at: <https://doi.org/10.1068/b35097>.
- Hewett, D.P. (2010) *Sound Propagation in an Urban Environment*. University of Oxford.
- Holpuch, J. (n.d.) *Olomouc founding legend - Romans in Olomouc*. Available at: <https://rimane.olomouc.eu/en/page/olomouc-founding-legend.html> (Accessed: 8 January 2024).
- Hong, D. *et al.* (2021) 'Interpretable Hyperspectral AI: When Non-Convex Modeling meets Hyperspectral Remote Sensing'. arXiv. Available at: <https://doi.org/10.48550/arXiv.2103.01449>.
- Hong, J.-H., Lu, Y.-H. and Chen, C.-H. (2019) 'The use of cctv in the emergency response: a 3d gis perspective', *The International Archives of the Photogrammetry, Remote Sensing and Spatial Information Sciences*, XLII-4-W15, pp. 19–25. Available at: <https://doi.org/10.5194/isprs-archives-XLII-4-W15-19-2019>.
- Hong, J.-H. and Tsai, C.-Y. (2020) 'Using 3D webGIS to support the disaster simulation, management, and analysis – examples of tsunami and flood.', *The International Archives of the Photogrammetry, Remote Sensing and Spatial Information Sciences*, XLIV-3-W1-2020, pp. 43–50. Available at: <https://doi.org/10.5194/isprs-archives-XLIV-3-W1-2020-43-2020>.
- Hron, V. and Halounová, L. (2019) 'Automatic reconstruction of roof models from building outlines and aerial image data', *Acta Polytechnica*, 59(5), pp. 448–457. Available at: <https://doi.org/10.14311/AP.2019.59.0448>.
- Hu, X. *et al.* (2013) 'Batch modeling of 3D city based on Esri cityEngine', in *IET International Conference on Smart and Sustainable City 2013 (ICSSC 2013)*. *IET International Conference on Smart and Sustainable City 2013 (ICSSC 2013)*, pp. 69–73. Available at: <https://doi.org/10.1049/cp.2013.1979>.
- Huang, H. *et al.* (2022) 'Estimating building height in China from ALOS AW3D30', *ISPRS Journal of Photogrammetry and Remote Sensing*, 185, pp. 146–157. Available at: <https://doi.org/10.1016/j.isprsjprs.2022.01.022>.
- Huang, Y. and Liu, W. (1997) 'Building the Estimation Model of Digitizing Error', *Photogrammetric Engineering and Remote Sensing* [Preprint]. Available at: <https://www.semanticscholar.org/paper/Building-the-Estimation-Model-of-Digitizing-Error-Huang-Liu/c74ff97acc21b6eac48a618229efbd749cba61ff> (Accessed: 2 January 2024).

- Information centre Olomouc (n.d.) *History of the town, Olomouc Tourism*. Available at: <https://tourism.olomouc.eu/en/historie/> (Accessed: 8 January 2024).
- Janga, B. *et al.* (2023) ‘A Review of Practical AI for Remote Sensing in Earth Sciences’, *Remote Sensing*, 15(16), p. 4112. Available at: <https://doi.org/10.3390/rs15164112>.
- Jenson, S.K. and Domingue, J.O. (1988) ‘Extracting Topographic Structure from Digital Elevation Data for Geographic Information System Analysis’, *PHOTOGRAMMETRIC ENGINEERING* [Preprint].
- Kleineberg, M. (2018) *Generating 3D roof meshes from aerial LIDAR data, Marian’s Blog*. Available at: <https://marian42.de/article/roofmeshes/> (Accessed: 4 January 2024).
- Kong, D., Xu, L. and Li, X. (2013) ‘A new method for building roof segmentation from airborne LiDAR point cloud data’, *Measurement Science and Technology*, 24(9), p. 095402. Available at: <https://doi.org/10.1088/0957-0233/24/9/095402>.
- Koppel, K. *et al.* (2017) ‘Sensitivity of Sentinel-1 backscatter to characteristics of buildings’, *International Journal of Remote Sensing*, 38, pp. 6298–6318. Available at: <https://doi.org/10.1080/01431161.2017.1353160>.
- Kucharczyk, M. *et al.* (2020) ‘Geographic Object-Based Image Analysis: A Primer and Future Directions’, *Remote Sensing*, 12(12), p. 2012. Available at: <https://doi.org/10.3390/rs12122012>.
- Kumar, M. and Bhardwaj, A. (2020) ‘Building Extraction from Very High Resolution Stereo Satellite Images Using OBIA and Topographic Information’, *Environmental Sciences Proceedings*, 5(1), p. 1. Available at: <https://doi.org/10.3390/IECG2020-08908>.
- Lang, S. (2008) ‘Object-based image analysis for remote sensing applications: modeling reality – dealing with complexity’, in T. Blaschke, Stefan Lang, and G.J. Hay (eds) *Object-Based Image Analysis: Spatial Concepts for Knowledge-Driven Remote Sensing Applications*. Berlin, Heidelberg: Springer (Lecture Notes in Geoinformation and Cartography), pp. 3–27. Available at: https://doi.org/10.1007/978-3-540-77058-9_1.
- Lao, J. *et al.* (2018) ‘Is OpenStreetMap suitable for urban climate studies?’, in. *OGRS2018, Open Source Geospatial Research & Education Symposium*. Available at: <https://shs.hal.science/halshs-01898612> (Accessed: 3 January 2024).
- lawinsider (n.d.) *Building footprint Definition, Law Insider*. Available at: <https://www.lawinsider.com/dictionary/building-footprint> (Accessed: 4 January 2024).
- Li, L. *et al.* (2020) ‘Roof Plane Segmentation from Airborne LiDAR Data Using Hierarchical Clustering and Boundary Relabeling’, *Remote Sensing*, 12(9), p. 1363. Available at: <https://doi.org/10.3390/rs12091363>.
- Li, Q. *et al.* (2018) ‘Hough Transform Guided Deep Feature Extraction for Dense Building Detection in Remote Sensing Images’, *2018 IEEE International Conference on Acoustics, Speech and Signal Processing (ICASSP)*, pp. 1872–1876. Available at: <https://doi.org/10.1109/ICASSP.2018.8461407>.
- Li, Q. *et al.* (2022) ‘Building Footprint Generation Through Convolutional Neural Networks With Attraction Field Representation’, *IEEE Transactions on Geoscience and Remote Sensing*, 60, pp. 1–17. Available at: <https://doi.org/10.1109/TGRS.2021.3109844>.

- Li, X. *et al.* (2020) ‘Developing a method to estimate building height from Sentinel-1 data’, *Remote Sensing of Environment*, 240, p. 111705. Available at: <https://doi.org/10.1016/j.rse.2020.111705>.
- Li, Z. *et al.* (2021) ‘A Deep Learning-Based Framework for Automated Extraction of Building Footprint Polygons from Very High-Resolution Aerial Imagery’, *Remote Sensing*, 13(18), p. 3630. Available at: <https://doi.org/10.3390/rs13183630>.
- Liu, T. and Yang, X. (2015) ‘Monitoring land changes in an urban area using satellite imagery, GIS and landscape metrics’, *Applied Geography*, 56, pp. 42–54. Available at: <https://doi.org/10.1016/j.apgeog.2014.10.002>.
- Liu, Z.J., Wang, J. and Liu, W.P. (2005) ‘Building extraction from high resolution imagery based on multi-scale object oriented classification and probabilistic Hough transform’, *Proceedings. 2005 IEEE International Geoscience and Remote Sensing Symposium, 2005. IGARSS '05*. [Preprint]. Available at: <https://doi.org/10.1109/igarss.2005.1525421>.
- Machete, R. *et al.* (2018) ‘The use of 3D GIS to analyse the influence of urban context on buildings’ solar energy potential’, *Energy and Buildings*, 177, pp. 290–302. Available at: <https://doi.org/10.1016/j.enbuild.2018.07.064>.
- Masson, V. *et al.* (2020) ‘City-descriptive input data for urban climate models: Model requirements, data sources and challenges’, *Urban Climate*, 31, p. 100536. Available at: <https://doi.org/10.1016/j.uclim.2019.100536>.
- Michelin, J.-C. *et al.* (2013) ‘Quality evaluation of 3D city building Models with automatic error diagnosis’, *The International Archives of the Photogrammetry, Remote Sensing and Spatial Information Sciences*, XL-7-W2, pp. 161–166. Available at: <https://doi.org/10.5194/isprsarchives-XL-7-W2-161-2013>.
- Michelin, J.-C., Mallet, C. and David, N. (2012) ‘Building edge detection using small-footprint airborne full-waveform lidar data’, *ISPRS Annals of the Photogrammetry, Remote Sensing and Spatial Information Sciences*, I-3, pp. 147–152. Available at: <https://doi.org/10.5194/isprsannals-I-3-147-2012>.
- Mohammadzadeh, K.K. (2020) *Automatic roof plane extraction from LiDAR data using RANSAC algorithm*. masterThesis. Fen Bilimleri Enstitüsü. Available at: <https://acikbilim.yok.gov.tr/handle/20.500.12812/473819> (Accessed: 4 January 2024).
- Müller, S. and Zaum, D. (2005) ‘Robust building detection in aerial images’, 36.
- National Geographic (n.d.) *Urbanization Effects, Environment*. Available at: <https://www.nationalgeographic.com/environment/article/urban-threats> (Accessed: 7 January 2024).
- Norman, M. *et al.* (2021) ‘Urban building detection using object-based image analysis (OBIA) and machine learning (ML) algorithms’, *IOP Conference Series: Earth and Environmental Science*, 620(1), p. 012010. Available at: <https://doi.org/10.1088/1755-1315/620/1/012010>.
- openstreetmap (2023) *History of OpenStreetMap - OpenStreetMap Wiki*. Available at: https://wiki.openstreetmap.org/wiki/History_of_OpenStreetMap (Accessed: 3 January 2024).
- Oskouee Aras, A., Babaei Aghdam, F. and Teymuri, I. (2023) ‘An analysis of modeling based on law and rules; City Engine software’, *Geography and Human Relationships*, 6(2), pp. 170–207. Available at: <https://doi.org/10.22034/gahr.2023.386685.1820>.

Overby, J. *et al.* (2004) 'Automatic 3D building reconstruction from airborne laser scanning and cadastral data using Hough transform', *International Archives of Photogrammetry, Remote Sensing and Spatial Information Sciences*, XXXIV.

Palacký University Olomouc (n.d.) *University History, Palacký University Olomouc*. Available at: <https://www.upol.cz/en/university/basic-information/university-history/> (Accessed: 8 January 2024).

Paliwal, S. *et al.* (2021) 'Digitize-PID: Automatic Digitization of Piping and Instrumentation Diagrams', in M. Gupta and G. Ramakrishnan (eds) *Trends and Applications in Knowledge Discovery and Data Mining*. Cham: Springer International Publishing (Lecture Notes in Computer Science), pp. 168–180. Available at: https://doi.org/10.1007/978-3-030-75015-2_17.

Parente, L. *et al.* (2019) 'Next Generation Mapping: Combining Deep Learning, Cloud Computing, and Big Remote Sensing Data', *Remote Sensing*, 11(23), p. 2881. Available at: <https://doi.org/10.3390/rs11232881>.

Prathiba, A.P. *et al.* (2020) 'Building Footprint Extraction from Very-High-Resolution Satellite Image Using Object-Based Image Analysis (OBIA) Technique', in J.K. Ghosh and I. da Silva (eds) *Applications of Geomatics in Civil Engineering*. Singapore: Springer (Lecture Notes in Civil Engineering), pp. 517–529. Available at: https://doi.org/10.1007/978-981-13-7067-0_41.

Qi, F., Zhai, J.Z. and Dang, G. (2016) 'Building height estimation using Google Earth', *Energy and Buildings*, 118, pp. 123–132. Available at: <https://doi.org/10.1016/j.enbuild.2016.02.044>.

Radio Prague International (2012) *Olomouc - a treasure trove of historical architecture, Radio Prague International*. Available at: <https://english.radio.cz/olomouc-a-treasure-trove-historical-architecture-8549441> (Accessed: 22 April 2024).

Rahaman, M.A., Kalam, A. and Al-Mamun, Md. (2023) 'Unplanned urbanization and health risks of Dhaka City in Bangladesh: uncovering the associations between urban environment and public health', *Frontiers in Public Health*, 11, p. 1269362. Available at: <https://doi.org/10.3389/fpubh.2023.1269362>.

Rastogi, K., Bodani, P. and Sharma, S.A. (2022) 'Automatic building footprint extraction from very high-resolution imagery using deep learning techniques', *Geocarto International*, 37(5), pp. 1501–1513. Available at: <https://doi.org/10.1080/10106049.2020.1778100>.

Rottensteiner, F. and Briese, C. (2003) 'Automatic generation of building models from LIDAR data and the integration of aerial images', *International Archives of the Photogrammetry, Remote Sensing and Spatial Information Sciences of the ISPRS*, 34.

Safonova, A. *et al.* (2023) 'Ten deep learning techniques to address small data problems with remote sensing', *International Journal of Applied Earth Observation and Geoinformation*, 125, p. 103569. Available at: <https://doi.org/10.1016/j.jag.2023.103569>.

Sahar, L. and Faust, N. (2013) 'An operational approach for building extraction from aerial imagery', *URISA Journal*, 25, pp. 47–52.

Sahin, H. *et al.* (2008) 'Comparison of object oriented image analysis and manual digitizing for feature extraction'.

Sampath, A. and Shan, J. (2008) 'Building roof segmentation and reconstruction from LiDAR point clouds using clustering techniques', *Int. Arch. Photogramm. Remote Sens. Spat. Inf. Sci.*, 37.

- San, D.K. and Turker, M. (2010) 'Building extraction from high resolution satellite images using hough transform', in. Available at: <https://www.semanticscholar.org/paper/BUILDING-EXTRACTION-FROM-HIGH-RESOLUTION-SATELLITE-San-Turker/4cc3e6fd43e1e3f54af27f3961d4d2cde630c7e6> (Accessed: 2 January 2024).
- Sanz-Ablanedo, E. *et al.* (2018) 'Accuracy of Unmanned Aerial Vehicle (UAV) and SfM Photogrammetry Survey as a Function of the Number and Location of Ground Control Points Used', *Remote Sensing*, 10(10), p. 1606. Available at: <https://doi.org/10.3390/rs10101606>.
- Šašek, M., Hlaváček, P. and Holub, J. (2019) 'Suburbanization processes of large cities in the Czech Republic in terms of migration', *Biblioteka Regionalisty*, (19), pp. 209–225. Available at: <https://doi.org/10.15611/br.2019.1.17>.
- Sedona, R. *et al.* (2019) 'Remote Sensing Big Data Classification with High Performance Distributed Deep Learning', *Remote Sensing*, 11(24), p. 3056. Available at: <https://doi.org/10.3390/rs11243056>.
- Senaratne, H. *et al.* (2016) 'A review of volunteered geographic information quality assessment methods', *International Journal of Geographical Information Science*, 31. Available at: <https://doi.org/10.1080/13658816.2016.1189556>.
- Singh, S., Jain, K. and Mandla, V.R. (2013) 'Image Based 3D Modeling of Campus (Department of Civil Engineering, IIT Roorkee, Uttarakhand, India) by Using SketchUp', in. Available at: [https://www.semanticscholar.org/paper/Image-Based-3D-Modeling-of-Campus-\(Department-of-by-Singh-Jain/ab23f6049280f84219bd26ee6f9aac64253c6191](https://www.semanticscholar.org/paper/Image-Based-3D-Modeling-of-Campus-(Department-of-by-Singh-Jain/ab23f6049280f84219bd26ee6f9aac64253c6191) (Accessed: 5 January 2024).
- Sketchup (n.d.) *3D Design Software | 3D Modeling on the Web, SketchUp*. Available at: <http://www.sketchup.com/page/homepage> (Accessed: 5 January 2024).
- Sohn, H.-G. *et al.* (2005) '3-D building extraction using IKONOS multispectral images', in *Proceedings. 2005 IEEE International Geoscience and Remote Sensing Symposium, 2005. IGARSS '05. Proceedings. 2005 IEEE International Geoscience and Remote Sensing Symposium, 2005. IGARSS '05.*, pp. 1432–1434. Available at: <https://doi.org/10.1109/IGARSS.2005.1525393>.
- Tarsha-Kurdi, F., Landes, T. and Grussenmeyer, P. (2007) 'Hough-Transform and Extended RANSAC Algorithms for Automatic Detection of 3D Building Roof Planes from Lidar Data', in. *ISPRS Workshop on Laser Scanning 2007 and SilviLaser 2007*, p. 407. Available at: <https://shs.hal.science/halshs-00264843> (Accessed: 4 January 2024).
- Tian, Y., Zhou, Q. and Fu, X. (2019) 'An Analysis of the Evolution, Completeness and Spatial Patterns of OpenStreetMap Building Data in China', *ISPRS International Journal of Geo-Information*, 8(1), p. 35. Available at: <https://doi.org/10.3390/ijgi8010035>.
- UNESCO (2000) 'Holy Trinity Column in Olomouc'. Available at: <https://whc.unesco.org/uploads/nominations/859rev.pdf>.
- Wang, C., Cho, Y.K. and Kim, C. (2015) 'Automatic BIM component extraction from point clouds of existing buildings for sustainability applications', *Automation in Construction*, 56, pp. 1–13. Available at: <https://doi.org/10.1016/j.autcon.2015.04.001>.
- Wasser, L. (2023) 'The Basics of LiDAR - Light Detection and Ranging - Remote Sensing | NSF NEON | Open Data to Understand our Ecosystems'. Available at: <https://www.neonscience.org/resources/learning-hub/tutorials/lidar-basics> (Accessed: 3 January 2024).

Wienert, S. *et al.* (2013) 'CognitionMaster: an object-based image analysis framework', *Diagnostic Pathology*, 8(1), p. 34. Available at: <https://doi.org/10.1186/1746-1596-8-34>.

wiki.gis.com (n.d.) *Slope - GIS Wiki | The GIS Encyclopedia*. Available at: <https://wiki.gis.com/wiki/index.php/Slope> (Accessed: 4 January 2024).

Wold, S. and Sandin, S. (2023) *Change is Deep: A Remote Sensing Perspective*. Available at: <https://urn.kb.se/resolve?urn=urn:nbn:se:liu:diva-194386> (Accessed: 2 January 2024).

World Bank (2023) *Overview, World Bank*. Available at: <https://www.worldbank.org/en/topic/urbandevelopment/overview> (Accessed: 5 November 2023).

Ying, S., Li, L. and Guo, R. (2011) 'Building 3D cadastral system based on 2D survey plans with SketchUp', *Geo-spatial Information Science*, 14(2), pp. 129–136. Available at: <https://doi.org/10.1007/s11806-011-0483-2>.

Zhang, S., Han, F. and Bogus, S.M. (2020) 'Building Footprint and Height Information Extraction from Airborne LiDAR and Aerial Imagery', pp. 326–335. Available at: <https://doi.org/10.1061/9780784482865.035>.

Zhuo, X. *et al.* (2018) 'Optimization of OpenStreetMap Building Footprints Based on Semantic Information of Oblique UAV Images', *Remote Sensing*, 10(4), p. 624. Available at: <https://doi.org/10.3390/rs10040624>.

ATTACHMENTS

Free attachments

Attachment 1: Map poster

Attachment 2: Thesis website

Microsoft Teams attachments

Attachment 3: Project files

Project file structure

Root directory	Subfolder	Content
Deliverables	City engine shapefiles	City City Multipatch3D Residential Residential Multipatch3D
	ESRI_GDB	City Residential Rurla
	DTM and Ortho Images	City DTM City Ortho image Residential DTM Residential Ortho image Rural DTM Rural Ortho image
	ProjectFiles	3DBuildings.aprx project
	Python notebook	Python notebooks for roof and height accuracy assessment
	Rule_file	CityEngine CGA script
	Sample_LAS	OLOMOUC 8-0_2.las